

# Human liver memory CD8<sup>+</sup> T cells utilise autophagy for tissue-residence

**Authors:** Leo Swadling<sup>1,6\*</sup>, Laura J Pallett<sup>1</sup>, Mariana Diniz<sup>1</sup>, Josephine M Baker<sup>1</sup>, Oliver E Amin<sup>1</sup>, Kerstin A Stegmann<sup>1</sup>, Alice R Burton<sup>1</sup>, Nathalie M Schmidt<sup>1</sup>, Anna Jeffery-Smith<sup>1,2</sup>, Nekisa Zakeri<sup>1</sup>, Kornelija Suveizdyte<sup>1</sup>, Farid Froghi<sup>3</sup>, Giuseppe Fusai<sup>3</sup>, William M Rosenberg<sup>3</sup>, Brian R Davidson<sup>3</sup>, Anna Schurich<sup>1,4</sup>, A Katharina Simon<sup>5</sup>, Mala K Maini<sup>1\*</sup>

## Affiliations:

<sup>1</sup> Division of Infection and Immunity, University College London, London, UK.

<sup>2</sup> Centre for Immunobiology, Blizard Institute, Barts and the London School of Medicine and Dentistry, QMUL, London, UK.

<sup>3</sup> Institute for Liver and Digestive Health, University College London, London, UK.

<sup>4</sup> Department of Infectious Diseases, Kings College London, London, UK.

<sup>5</sup> The Kennedy Institute of Rheumatology, NDORMS, University of Oxford, Oxford, UK.

<sup>6</sup> Lead contact

\* Correspondence: l.swadling@ucl.ac.uk & m.maini@ucl.ac.uk

## Summary

Tissue-resident memory T cells play critical roles in long-term pathogen and tumor immune-surveillance in the liver. We investigated the role of autophagy in equipping human memory T cells to acquire tissue-residence and maintain functionality in the immunosuppressive liver environment. By performing *ex vivo* staining of freshly isolated cells from human liver tissue we found that an increased rate of basal autophagy is a hallmark of intrahepatic lymphocytes, particularly liver-resident CD8<sup>+</sup> T cells. CD8<sup>+</sup> T cells with increased autophagy were those best able to proliferate and mediate cytotoxicity and cytokine production. Conversely, blocking autophagy induction resulted in the accumulation of depolarised mitochondria, a feature of exhausted T cells. Primary hepatic stellate cells, or the prototypic hepatic cytokine IL15, induced autophagy in parallel with tissue-homing/retention markers. Inhibition of T cell autophagy abrogated tissue-residence programming. Thus, upregulation of autophagy adapts CD8<sup>+</sup> T cells to combat mitochondrial depolarisation, optimise functionality, and acquire tissue-residence.

## Introduction

The liver has a distinct tolerogenic immune environment that is exploited by hepatotropic infections and primary and metastatic tumors. With deaths due to viral hepatitis now exceeding those resulting from tuberculosis, malaria, and HIV (Graber-Stiehl 2018), and primary liver cancer predicted to rise to the 13<sup>th</sup> leading cause of death worldwide by 2040 (Foreman et al. 2018), it is essential that we gain a better understanding of liver immunity to aid development of immunotherapies.

T cells play an important role in clearing virus-infected and cancerous cells, but they require tight regulation to avoid immunopathology. Many T cell tolerising mechanisms are present in the liver (reviewed in (Maini & Pallett 2018)) to avoid an excessive immune response to the constant flow of microbial products and diet derived-antigens entering the liver from the gut via the portal vein (Protzer et al. 2012). The liver is also unique in that the majority of its blood supply is venous and, therefore, relatively low in oxygen and flow rate when compared to arterial blood (reviewed in (Carreau et al. 2011)), and key T cell metabolites may be depleted within the liver microvasculature (Pallett et al. 2015; Das et al. 2008). However, little is known about the T cell-intrinsic adaptations required to survive and retain functionality in the liver.

We have recently defined a population of CD8<sup>+</sup> tissue-resident memory T cells (T<sub>RM</sub>), which reside in the liver without recirculating through the blood, and that are preferentially expanded in patients with well-controlled hepatitis-B virus (HBV) infection (Pallett et al. 2017). Liver-resident T<sub>RM</sub> have a distinct phenotype, transcription factor expression, and the capacity to maintain efficient IL2 and IFN $\gamma$  production in the tolerogenic liver, but the cellular processes and metabolic state driving these adaptations have not been defined (Fernandez-Ruiz et al. 2016; Tse et al. 2011).

One constitutive but highly dynamic cellular process that all cells require, and that is regulated to maintain homeostasis under cellular stress, is Macroautophagy (subsequently referred to here as autophagy). Autophagy is a highly conserved lysosome-mediated intracellular bulk recycling process (Clarke & Simon 2019). The nucleation of double membrane vesicles, called autophagosomes, facilitates engulfment of a portion of the cytoplasm for delivery to the lysosome for degradation (Clarke & Simon 2019). Autophagy has two main roles: firstly, it allows cells to maintain their cellular homeostasis, by removing unwanted cytoplasmic content (pathogens, protein aggregates, damaged organelles, reactive oxygen species [ROS]); secondly, it provides biomolecules for cellular metabolism through the catabolism of proteins and complex lipids. The importance of this cellular process to diverse human T cell memory subsets, including  $T_{RM}$ , is not known.

Here we address the hypothesis that liver-resident T cells utilise higher constitutive autophagy levels to maintain homeostasis in the liver. We characterise autophagy levels in human memory T cell subsets, including liver-resident T cells and hepatitis-B virus-specific T cells. Making use of our regular access to fresh human liver samples, we show that intrahepatic lymphocytes have a higher *ex vivo* level of autophagy, with lymphocytes that reside long term in the liver showing the highest rates of autophagy ( $T_{RM}$  and mucosal associated invariant T cells; MAITs). Recirculating T cells specific for the hepatotropic infection HBV also show high levels of autophagy. Recently activated, proliferating, or highly functional T cells have enhanced rates of autophagy, and maintenance of mitochondrial fitness is lost upon treatment with autophagy inhibitors. Finally, we show that the prototypical liver cytokine IL15, required for the induction of liver-resident T cells, can also upregulate T cell autophagy, whereas blockade of autophagy abrogates  $T_{RM}$  programming of  $CD8^+$  T cells.

## Results

### *Higher ex vivo autophagy levels are characteristic of intrahepatic lymphocytes*

To measure autophagy in human T cells we employed an established flow cytometry based assay (FlowCelect Autophagy LC3 antibody-based kit, Merck Millipore/Luminex (Eng et al. 2010)) that has been previously applied to human and murine lymphocyte subsets (O’Sullivan et al. 2016; Clarke et al. 2018), in particular T cells (Puleston et al. 2014; Kabat et al. 2016; Sanderson & Simon 2017). A reliable and specific marker of autophagic vesicles (autophagosomes) is LC3 (microtubule-associated protein 1 light chain 3) - a cytosolic protein that is lipidated and then incorporated into *de novo* generated autophagosomes (Klionsky et al. 2016). To assay basal autophagy levels, cells are selectively permeabilised to extract cytosolic LC3-I, then autophagosome-bound LC3-II is detected using a fluorescently labelled anti-LC3 antibody (“unblocked”; see methods). We also measured the accumulation of autophagosomes over time by inhibiting autophagosome breakdown with bafilomycin A1 (bafA1), an endosomal acidification inhibitor (Klionsky et al. 2016) (“blocked data”). Finally, as a proxy for autophagic flux, and to eliminate the variation in the number of autophagosomes at baseline (including tissue-specific variation and cell size), we calculated the ratio of LC3 staining for blocked vs. unblocked samples.

We first investigated whether lymphocytes that have been exposed to the tolerogenic liver microenvironment display a different level of autophagy to peripheral lymphocytes isolated from blood. To do so we assayed the level of autophagy in human intrahepatic lymphocytes (IHL) from explanted liver samples, liver perfusates, and paired blood (peripheral blood mononuclear cells, PBMC). To observe the relative autophagy levels of all lymphocyte subsets from paired

PBMC and IHL samples we performed dimension reduction by tSNE (t-Distributed Stochastic Neighbor Embedding) on multiparametric flow cytometry data to visualise the relative LC3 intensity of each cell. PBMC and IHL showed overlapping distributions but overall the intensity of LC3 staining was higher on IHL (**Figure 1a**; gating and example plots **Figure S1a**). Several clusters of lymphocytes with high intensity LC3 staining were uniquely observed in IHL samples. We therefore extended this analysis to a larger cohort of paired human blood and liver samples. Intrahepatic T cells had a significantly higher *ex vivo* level of autophagy than T cells isolated from blood when gating on CD4<sup>+</sup>, CD8<sup>+</sup>, or total CD3<sup>+</sup> T cells (**Figure 1b**; unblocked data (no bafA1) and blocked/unblocked ratio in **Figure S1b-c**). Although autophagy levels increased with T cell granularity (SSC, Side SCatter), they did not directly correlate with T cell size (FSC, Forward SCatter), and enhanced *ex vivo* autophagy levels were not higher as a result of T cells showing a different morphology in the liver (**Figure S1a**). Differences in autophagy levels between blood and liver were also not attributable to differences in sample processing, since they were maintained when using IHL isolated from perfusion fluid or healthy transplant livers, which are processed identically to blood (**Figure S1d**).

Mucosal associated invariant T cells (MAITs; CD161<sup>hi</sup> Vα7.2<sup>+</sup>), a population of T cells which has recently been shown to reside long-term in the liver (Salou et al. 2019), also had higher levels of autophagy when compared to CD161<sup>mid</sup> or CD161<sup>-</sup> T cells in the blood or liver, with each of these subsets having higher LC3 levels in the liver than their circulating counterparts (**Figure 1c**). Other lymphocytes assayed also had a higher level of autophagy in the liver when compared to the equivalent population in the blood, including CD19<sup>+</sup> B cells (**Figure 1d**). CD56<sup>+</sup> Natural killer cells (NK) were the exception, where autophagy levels were comparable

between peripheral and intrahepatic populations (**Figure 1d**). Overall, several lymphocyte subsets isolated from the liver had a higher level of autophagy than their counterparts isolated from blood, in particular T cells.

***Enhanced autophagy by intrahepatic T cells is not a result of a difference in T cell memory subset frequency or recent proliferation***

We investigated whether the difference in T cell autophagy levels in the liver and blood are due to a different T cell subset composition in the two compartments. In both IHL and PBMC, CD8<sup>+</sup> T cells with an effector memory (T<sub>EM</sub>, CCR7<sup>-</sup>CD45RA<sup>-</sup>) or central memory (T<sub>CM</sub>; CCR7<sup>+</sup>CD45RA<sup>-</sup>) phenotype had the highest level of autophagy, with naïve (CCR7<sup>+</sup>CD45RA<sup>+</sup>) and terminally differentiated effector memory (T<sub>EMRA</sub>; CCR7<sup>-</sup>CD45RA<sup>+</sup> (Sallusto et al. 1999) T cells showing lower levels (**Figure 2a**). The liver is enriched for memory T cells and has few naïve T cells relative to blood (Pallett et al. 2017), however, all T cell subsets had a higher level of autophagy in the liver, indicating that differences between these compartments were not purely due to a different balance of T cell memory subsets (**Figure 2b**).

Autophagy is enhanced when murine (Hubbard et al. 2010; Kabat et al. 2016; Watanabe et al. 2014; Botbol et al. 2015; Yang et al. 2013) and human T cells are activated and proliferating (Watanabe et al. 2014). If the liver housed a larger proportion of proliferating T cells this may explain their higher autophagy levels. The percentage of CD8<sup>+</sup> T cells expressing Ki67, a marker of recent cell cycling, was not significantly higher on T cells within the liver than the circulation (**Figure 2c-d**; (Pallett et al. 2017)). We confirmed in humans that *ex vivo* proliferating (Ki67<sup>+</sup>) CD8<sup>+</sup> T cells in both blood and liver had higher autophagy levels than Ki67<sup>-</sup> CD8<sup>+</sup> T cells

(**Figure 2d-e**), and that recently activated (**Figure 2e**) and dividing human CD8<sup>+</sup> T cells (**Figure 2f**) showed upregulated autophagy, as has been shown previously in mice (Hubbard et al. 2010; Pua et al. 2007). We conclude that T cells in the liver show enhanced autophagy levels relative to their counterparts in the blood that cannot be accounted for solely by their differentiation or proliferation status.

### ***Autophagy levels are highest in T cells that reside long-term in the liver***

We have recently defined a population of CD8<sup>+</sup> T cells that persist long-term and maintain functionality in the immunosuppressive liver environment (Pallett et al. 2017). These liver-resident CD8<sup>+</sup> T cells are distinguished by expression of the tissue retention markers CD69 (a sphingosine 1-phosphate receptor-1 antagonist) with or without CD103 (integrin $\alpha$ E, which in combination with integrin $\beta$ 7 can bind to E-cadherin on endothelial cells and hepatocytes). CD69<sup>+</sup>CD103<sup>+/-</sup> T<sub>RM</sub> are enriched in the liver, with CD69<sup>+</sup>CD103<sup>+</sup> being completely absent from the blood (example plot in **Figure S1a**; (Pallett et al. 2017; Stelma et al. 2017)).

We assessed the rate of autophagy within the liver-resident CD8<sup>+</sup> T<sub>RM</sub> compared to non-resident, liver-infiltrating T cells (CD69<sup>-</sup>CD103<sup>-</sup>) transiting through the liver at the time of sampling. By looking more closely at the subpopulations of CD8<sup>+</sup> T cells in the tSNE output we observed that CD69<sup>+</sup>CD103<sup>+/-</sup> CD8<sup>+</sup> T<sub>RM</sub> clustered together in areas of high LC3 expression relative to all PBMC and IHL (**Figure 3a**). Extending these data to a cohort of 38 paired human blood and liver samples, a step-wise increase in autophagy levels was seen from CD69<sup>-</sup>CD103<sup>-</sup> liver-infiltrating, to CD69<sup>+</sup>CD103<sup>-</sup>, to CD69<sup>+</sup>CD103<sup>+</sup> liver-resident memory CD8<sup>+</sup> T cells, suggesting

that rates of autophagy are highest in populations of T cells that reside long-term in the liver (**Figure 3b-c**; Ratio blocked vs. unblocked, **Figure S2a**).

We next tested whether the *ex vivo* difference in autophagy rates in human liver-resident memory CD8<sup>+</sup> T cells could be validated using two further markers of autophagosomes and by imaging flow cytometry. We found that CD8<sup>+</sup> T<sub>RM</sub> are also characterised by higher autophagy levels when quantifying the relative accumulation of the autophagosome-associated cargo protein sequestosome-1 (p62, SQSTM1; **Figure S2b**) and using the autophagic vesicle-specific dye Cyto-ID (**Figure S2c-d**; example plot **Figure S1a**). To directly visualise autophagosomes within T cells we then used a recently developed autophagy assay employing imaging flow cytometry (ImageStream; (Klionsky et al. 2016; Phadwal et al. 2012; Puleston et al. 2014)) to visualise LC3 within autophagosome puncta (gating strategy and staining controls **Figure S3**). We confirmed by ImageStream that there was a higher per-cell median fluorescence of LC3, representing a higher total number of autophagosomes (example cell images **Figure 3d**), for liver-resident T cells relative to peripheral CD8<sup>+</sup> T cells or liver-infiltrating T cells (**Figure 3e**). We then quantified distinct autophagosomes as LC3<sup>+</sup> puncta within T cells and showed that the majority of T<sub>RM</sub> contained multiple autophagosome puncta, whereas recirculating CD8<sup>+</sup> in the liver mainly contained 1 or no autophagosomes (**Figure 3f**). Taken together, these data using four different approaches, showed enhanced autophagy levels in CD8<sup>+</sup> T cells that are resident versus those infiltrating the liver or in the periphery.

Using PBMC isolated from patients chronically infected with hepatitis B virus (**Table S1**) we next asked whether a population of memory T cells that has been primed and/or encountered



cognate antigen within the liver would also be imprinted with enhanced autophagy levels. We stained PBMC with MHC-class I dextramers loaded with peptides corresponding to immunodominant hepatitis-B virus (HBV) and cytomegalovirus (CMV) epitopes in HLA-A\*02<sup>+</sup> patients and compared the autophagy levels of total CD8<sup>+</sup> T cells, HBV-specific T cells, and a population of memory T cells directed against a control virus (CMV-specific). HBV-specific T cells showed a higher level of autophagy than total CD8<sup>+</sup> T cells or CMV-specific T cells assayed in the same patients (**Figure 3g**). The small population of HBV-specific memory T cells with high levels of autophagy that persists in patients chronically infected with HBV may represent a pool of T cells that have enhanced autophagy levels imprinted on them whilst in the liver. Taken together, these data show that autophagy levels are highest in T cell subsets resident or encountering antigen within the liver.

***Enhanced autophagy levels are associated with enhanced effector function and mitochondrial fitness in T cells***

We next investigated the functional consequence of enhanced autophagy for human CD8<sup>+</sup> T cells to determine whether the T cells that gain specific effector functions on activation are also those that have the highest induction of autophagy.

Upon *in vitro* activation, CD8<sup>+</sup> T cells that produced IFN $\gamma$  also showed an enhanced rate of autophagy (**Figure 4a-b**; LC3 staining and cytokine release controls are shown in **Figure S3e**; LC3 staining by FlowCelect kit was performed in parallel to brefeldin A treatment and permeabilisation with transcription factor staining kit to confirm that autophagosome quantitation was equivalent by intracellular staining,  $r = 0.9404$   $p < 0.0001$  for CD8<sup>+</sup> T cells;

**Figure S3f).** Without stimulation, T cells with cytolytic potential *ex vivo* also had higher autophagy levels than T cells that lacked perforin or granzyme B expression (GzB; **Figure 4c**). When stimulated, the expanded population of CD8<sup>+</sup> T cells expressing cytolytic markers showed an increase in autophagy, and T cells that co-expressed GzB and perforin were those with the highest autophagy levels (**Figure 4d**). There is, therefore, an association on a per-cell basis between the upregulation of autophagy by human CD8<sup>+</sup> T cells upon activation and the acquisition of T cell effector functions.

Murine T cells lacking autophagy due to ATG7 deletion have been shown to accumulate mitochondrial mass and reactive oxygen species (ROS) (Puleston et al. 2014); a higher level of autophagy promotes removal of depolarised mitochondria and ROS in T cells (mitophagy; (Schlie et al. 2015; Jia & He 2011; Pua et al. 2009; Stephenson et al. 2009; Hubbard et al. 2010). This may be particularly important in an oxygen deprived environment, such as the liver, where mitochondrial damage and ROS accumulation can be high, as has been shown for HBV-specific T cells (Fisicaro et al. 2017; Schurich et al. 2016).

To assess mitochondrial fitness we co-stained T cells with MitoTracker Deep Red (MtDR), a polarisation sensitive dye that only stains functional polarised mitochondria, and MitoTracker green (MtG) which stains all mitochondria (Puleston 2015; Zinser et al. 2018). Dying T cells in the liver and blood (defined as fixable live/dead<sup>+</sup>) were almost exclusively MtDR<sup>lo</sup>, consistent with the high rates of depolarised mitochondria expected in this population (**Figure S4a**). Within the live lymphocyte gate a larger proportion of total CD8<sup>+</sup> T cells had depolarised mitochondria in the liver than in the blood (**Figure 4e**). When dissected by expression of tissue-residency

markers, the liver-infiltrating CD69<sup>+</sup>CD103<sup>+</sup> fraction had the highest burden of dysfunctional mitochondria (**Figure 4f**), in line with their lower autophagy rate compared to T<sub>RM</sub>. When autophagy was blocked overnight using the autophagy specific inhibitor of ULK1/2 (Unc-51 like autophagy activating kinase; blocking autophagosome nucleation (Petherick et al. 2015)) MRT68921 dihydrochloride, all liver T cell subsets accumulated depolarised mitochondria, underscoring the importance of this pathway for removal of damaged mitochondria, as has been shown for murine T cells (**Figure 4g**; (Pua et al. 2009; Watanabe et al. 2014; Stephenson et al. 2009)). Enhanced accumulation of depolarised mitochondria was also seen using endosomal acidification inhibitors to block autophagosomal digestion (bafA1 or reagent A, FlowCollect Kit, **Figure 4g**). Consistent with their lower baseline autophagy levels, with each autophagy inhibitor it was again the infiltrating rather than resident fraction of intrahepatic CD8<sup>+</sup> T cells that accumulate the highest levels of depolarised mitochondria (**Figure 4g**).

One potential caveat to these findings is that a subpopulation of CD8<sup>+</sup> T<sub>RM</sub> with the ability to efflux fluorescent dyes such as MtG has been previously described in the human lung, spleen, and bone marrow (Kumar et al. 2018). We found that efflux<sup>+</sup> T cells were also present in the human liver and are enriched within the CD69<sup>+</sup>CD103<sup>±</sup> T<sub>RM</sub> fractions (**Figure S4b**). However, when efflux pumps inhibitors verapamil or cyclosporin A (CSA) were used the percentage of depolarised mitochondria (MtDR<sup>lo</sup>) did not change (**Figure S4c**), showing that efflux<sup>+</sup> T<sub>RM</sub> were retained within the MtDR<sup>+</sup> gate independently of dye efflux. Therefore, the differences in depolarised mitochondria that we observed were not simply due to differential dye efflux. The accumulation of depolarised mitochondria can also be a general feature of apoptosis, however, the viability of lymphocytes treated with autophagy inhibitors overnight was not greatly reduced

relative to untreated cells (**Figure S5**). This suggests that the accumulation of depolarised mitochondria was a consequence of a reduction in mitophagy and not secondary to any toxicity of the autophagy inhibitors.

Overall these data suggest that the liver is an environment in which mitochondrial damage is high, and where persistent high levels of mitophagy may be required for T cells to adapt to residency within this milieu.

***In vitro induced  $T_{RM}$  have a high level of autophagy, and  $T_{RM}$  induction is limited when autophagy is blocked***

Tissue-resident T cells have only recently been recognised and the mechanism by which residency is imprinted on T cells *in vivo* is yet to be fully decoded. We and others have previously tested a range of cytokines and T cell stimulations and identified an efficient protocol to induce CD8<sup>+</sup>  $T_{RM}$  phenotype T cells *in vitro* from human PBMC using sequential exposure to IL15 and then TGFβ (Pallett et al. 2017; Sowell et al. 2017; Mackay et al. 2015), two prototypical liver cytokines. These *de novo* ‘induced residency’ CD8<sup>+</sup>  $T_{RM}$  express both CD69 and CD103 and have several other characteristics of human liver-resident T cells (e.g. expression of CXCR3, CXCR6, and a Blimp<sup>hi</sup>Eomes<sup>lo</sup> phenotype (Pallett et al. 2017)). Here we used this protocol to assess whether *in vitro* induced residency is also accompanied by enhanced level of autophagy, consistent with  $T_{RM}$  staining *ex vivo*. Sequential exposure to IL15 and TGFβ, shown to optimally induce *de novo* CD8<sup>+</sup> CD69<sup>+</sup>CD103<sup>+</sup>  $T_{RM}$  from PBMC (Pallett et al. 2017) was also able to efficiently upregulate autophagy, with the latter effect attributable to IL15 (**Figure 5a-b**). We confirmed that IL15 alone induced autophagy in a dose-dependent manner in CD8<sup>+</sup> T cells

either within PBMC or after isolation; this autophagy induction could be blocked with an anti-IL15 monoclonal antibody (**Figure 5b**).

IL15 is constitutively expressed by several liver resident cell types, including hepatic stellate cells (HSCs)(Golden-Mason et al. 2004; Winau et al. 2007; Zhou et al. 2018) and liver macrophage populations (Golden-Mason et al. 2004). To test whether a liver-resident cell population known to produce IL15 could recapitulate the high levels of T cell autophagy observed in liver T<sub>RM</sub>, we co-cultured peripheral T cells with primary HSCs isolated from healthy margins of liver resections. A trend towards a dose-dependent induction of T cell autophagy was observed following incubation of T cells with HSCs and this induction could be partially blocked by the addition of recombinant human IL15R $\alpha$  (**Figure 5c**), supporting a potential role for HSC-derived IL15 in driving the high T cell autophagy we observed in human IHL.

To investigate whether the induction of autophagy was a prerequisite for the acquisition of a T<sub>RM</sub> profile, we used inhibitors of autophagy during the cytokine T<sub>RM</sub> induction protocol. The autophagy inhibitors MRT69821 dihydrochloride and 3-MA (3-Methyladenine; a type I and III Phosphatidylinositol 3-kinases inhibitor (Mocholi et al. 2018)) were able to partially block the induction of autophagy seen during *in vitro* T<sub>RM</sub> induction (**Figure 5d-e**). Crucially, the reduction in autophagy achieved with these inhibitors abrogated the acquisition of molecules critical for tissue retention (**Figure 5f, Figure S5d**).

The observed abrogation of T<sub>RM</sub> induction was not attributable to autophagy inhibitors rendering T cells completely unresponsive to stimulation nor to a loss of T cell viability. Inhibition of autophagy selectively prevented *in vitro* T<sub>RM</sub> induction by IL15/TGF $\beta$  without causing a significant reduction in the number of liver-infiltrating CD69<sup>+</sup>CD103<sup>+</sup> T cells (**Figure S5d**) or in

T<sub>RM</sub> cell viability (**Figure S5e**). T cells could still become activated (co-expression of CD38 and PD-1) and differentiate into effectors (CD27<sup>+</sup>CD28<sup>-</sup>) when TCR-stimulated in the presence of autophagy inhibitors (**Figure 5g**). Overall, these data suggest that IL15-driven induction of T cell autophagy may be specifically required for tissue-residency programming.

## Discussion

Using high dimensional flow and imaging cytometry applied to fresh human liver samples we show a link between higher utilisation of autophagy and tissue-resident memory. We show that enhanced autophagy is also required for optimal acquisition of tissue residency *in vitro* and maintenance of T cell mitochondrial fitness, and may be imprinted on liver-resident CD8<sup>+</sup> T cells by the prototypic hepatic cytokine IL15.

Autophagy plays an active role in the functionality and differentiation of diverse lymphocyte subsets, in particular for long-lived and quiescent cells (Riffelmacher et al. 2018; Clarke et al. 2018; Zhu et al. 2018). Complete ablation of autophagy in total murine T cells results in defective homeostasis or responsiveness to stimulation (Schlie et al. 2015; Puleston et al. 2014; Stephenson et al. 2009; Pua et al. 2009; Jia & He 2011; Hubbard et al. 2010). In particular, autophagy-deficient memory T cells are depleted, either because they fail to survive the transition from effector to memory T cells or because they need autophagy for their maintenance (Schlie et al. 2015; Xu et al. 2014; Puleston et al. 2014; Murera et al. 2018; DeVorkin et al. 2019); however, how varied levels of autophagy impact on T cell survival, functionality, and differentiation and the importance of autophagy for human T cell subsets, in particular tissue-resident CD8<sup>+</sup> T cells had not been considered.

Not only were autophagy levels high in total CD3<sup>+</sup>, CD4<sup>+</sup>, or CD8<sup>+</sup> T cells isolated from human liver samples, but within the intrahepatic compartment the T cells with the highest level of autophagy were those that express the tissue-retention markers CD69<sup>+</sup> and CD103<sup>+</sup> (Pallett et al. 2017). We demonstrated that differences between T cells in the liver and blood were not solely due to differences in intrahepatic T cell morphology, memory subsets composition, or levels of activation and proliferation.

Conceptually, how might human T cells in the liver benefit from enhanced autophagy levels? We first tried to address this by asking if the levels of autophagy in T cells are linked to their functional profile, as has been suggested in mice. In mice, autophagy may be transiently reduced immediately after T cell activation but effector T cells show a higher level of autophagic flux than naïve T cells and complete abrogation of autophagy has a profound effect on T cell survival and transitioning to long-lived memory T cells (Xu et al. 2014). We confirmed that autophagy was increased in effector T cells 3-5 days post-T cell receptor (TCR)-mediated activation and further demonstrated that on a per-cell basis the acquisition of T cell effector function only occurred in accordance with increased rates of autophagy.

*Ex vivo* expression of cytolytic mediators or the proliferation marker Ki67 correlated with higher levels of autophagy. Higher levels of autophagy may, therefore, be required to allow a T cell to respond to stimulation, or to switch on and retain effector functions. This is supported by murine data showing that anergy is induced in CD4<sup>+</sup> T cells if autophagy is inhibited at the time of TCR-mediated stimulation (Mocholi et al. 2018). This was also the case in our *in vitro* T<sub>RM</sub> induction model, which showed that the pro-proliferative cytokine IL15 drives CD8<sup>+</sup> T cell autophagy in a dose-dependent manner.

Autophagy is the main mechanism by which damaged depolarised mitochondria are selectively targeted to the lysosome for their removal (mitophagy; (Villa et al. 2018)) and this pathway has been shown to be important in neutrophils (Riffelmacher et al. 2018), B cells (Clarke et al. 2018) and global murine T cells (Pua et al. 2009; Stephenson et al. 2009; Jia & He 2011; Murera et al. 2018). T cell-specific autophagy knockout models uniformly demonstrate an increase in depolarised mitochondria and ROS, leading to increased T cell death (Murera et al. 2018; Jia & He 2011; Pua et al. 2009; Stephenson et al. 2009; Watanabe et al. 2014; Schlie et al. 2015). Mitochondria can become damaged when defective mitochondrial proteins or ROS accumulate (reviewed in (Haynes et al. 2013)). The liver is unique in that it receives the majority of its blood as deoxygenated venous blood (Carreau et al. 2011) and is characterised by high levels of oxidative stress (Huang et al. 2017; García-Ruiz & Fernández-Checa 2018). Of note, mitochondrial defects and reduced survival are also a characteristic of autophagy-deficient hepatic stellate cells (Hernándezgea et al. 2012).

Our study showed that intrahepatic T cells accumulate depolarised mitochondria *ex vivo*, in keeping with the high oxidative stress milieu. Pharmacological inhibition of autophagy in human T cells can also lead to an accumulation of damaged mitochondria, suggesting a role of mitophagy in the maintenance of human T cell homeostasis. Liver-resident T cells with high basal autophagy were better able to maintain mitochondrial fitness. Our data suggest that non-resident T cells that infiltrate the liver are less well-adapted to the milieu and, without the requisite high basal autophagy levels, are more susceptible to mitochondrial depolarisation. Similarly we found that MAITs, another liver resident population (Salou et al. 2019) previously shown to maintain tight control of depolarised mitochondria (Zinser et al. 2018), are also



characterised by high autophagy levels. Overall, these observations support the concept that tight mitochondrial quality control is essential for T cell homeostasis in the liver and that this is provided by enhanced autophagy levels. Future work is needed to investigate whether the depolarised mitochondria characteristic of liver T<sub>RM</sub> are accompanied by a high burden of cytosolic or mitochondrial ROS, and whether ROS scavengers can abrogate their dependence on autophagy (Fisicaro et al. 2017; Pilipow et al. 2015). Alternatively, the requirement for mitophagy to replace damaged mitochondria may provide a ROS-independent mechanism by which autophagy adapts T cells to tissue-residence.

A loss of control of mitochondrial fitness is a characteristic of exhausted T cells (Bensch et al. 2016), in particular HBV-specific T cells (Schurich et al. 2016). Exhausted HBV-specific T cells could be partially rejuvenated *in vitro* by correcting this mitochondrial defect with mitochondria-specific ROS scavengers (Fisicaro et al. 2017). Using MHC class I multimers we were able to show that HBV-specific T cells circulating in chronically infected patients, that would have been primed and/or exposed to cognate antigen in the liver, had a higher level of autophagy when assayed in the blood relative to total CD8<sup>+</sup> T cells or CMV-specific T cells. This suggested that virus-specific T cells can have enhanced autophagy levels imprinted on them by the environment in which they encounter antigen.

We investigated the autophagy inducing properties of the prototypic liver cytokine IL15 (Golden-Mason et al. 2004; Jiao et al. 2016) which can be produced by HSCs and hepatic macrophages (Golden-Mason et al. 2004; Winau et al. 2007; Zhou et al. 2018). IL15 has been linked to the maintenance and imprinting of T<sub>RM</sub>-phenotype (Holz et al. 2018; Mackay et al. 2015) and to autophagy induction in NK and NKT cells (Zhu et al. 2018). In this study we show

that IL15 can directly induce autophagy in human T cells and that T<sub>RM</sub> induction *in vitro* is dependent on autophagy. IL15 has also been used for optimal expansion of antigen specific T cells *in vivo* in melanoma models (Zeng et al. 2005), for stem-cell like chimeric antigen receptor T cells (Tscm)(Hurton et al. 2016), and is crucial for persistence of inflationary MCMV-specific T cells (Baumann et al. 2018). We have previously shown that IL15 in combination with IFN $\alpha$  can restore T cell effector function and proliferative capacity in exhausted HBV-specific T cells *in vivo* for mice and *in vitro* for humans (Di Scala et al. 2016). Whether autophagy is involved in shaping T cell differentiation and functionality in these settings should be investigated. Taken together, our data suggest that IL15 or other means of inducing T cell autophagy may constitute a useful strategy to promote highly functional T cells with the capacity to reside in the liver and resist mitochondrial depolarisation, for example in the optimisation of adoptive T cell therapy for HCC (Qasim et al. 2015).

In summary, upregulation of autophagy in human liver-resident CD8<sup>+</sup> memory T cells drives the acquisition of tissue retention markers and protects against mitochondrial depolarisation to optimise effector function. We demonstrate the capacity of the prototypic hepatic cytokine IL15 to induce autophagy and suggest this imposes a cell-intrinsic adaptation to the liver niche on tissue-resident memory T cells.

---

## Acknowledgments

We are extremely grateful to all patients and control volunteers who participated in this study and to all clinical staff who helped with recruitment, in particular those working with the Tissue Access for Patient Benefit project (TAPb) at The Royal Free Hospital, London, UK. This work

was funded by a Wellcome Trust Senior Investigator Award (101849/Z/13/A) to MKM and a Medical Research Foundation grant (MRF-044-0001-RG-SWADL) to LS.

### **Author Contributions**

MKM and LS conceived the project and obtained funding. LS, AKS and MKM designed experiments. LS, MD, LJP and JB generated data. LS, JB AKS and MKM analysed and interpreted data. LS, LJP, OEA, KAS, ARB, NS, AJS, NZ, KS, FF, GF, WMR, BRD and AS provided or processed essential patient samples and clinical data. LS and MKM prepared the manuscript. All authors provided critical review of the manuscript. We are very grateful to Jamie Evans at the Rayne Building FACS facility for assistance with Flow cytometry assays and to Prabhjoat Chana at Merck group for assistance with ImageStream experiments.

**Declaration of interests:** Authors declare no competing financial interests, consulting positions or patents. The Maini lab has received unrestricted research grants from Gilead Science inc, Roche, and Immunocore.

### **Figure 1. Intrahepatic lymphocytes are characterised by high *ex vivo* autophagy levels; (a)**

The dimensionality reduction algorithm tSNE was applied to flow cytometry data (single cell expression values from total live CD45<sup>+</sup> singlet lymphocytes for: CD3, CD4, CD8 $\alpha$ , CD19, CD103, CD69, pan- $\gamma\delta$  T cell receptor (TCR), pan- $\alpha\beta$  TCR, CD161, CD56, LC3) to generate a two-dimensional map of lymphocytes from paired PBMC (left) and IHL (middle) samples from two individuals coloured by intensity of LC3 or by lymphocyte subset (right; example gating **Figure S1a**). **(b)** Histograms (gated on CD8<sup>+</sup>; +/- bafilomycin A1 [bafA1] treatment, 0.1  $\mu$ M; FMO for LC3)) and summary data for LC3 staining of paired peripheral (PBMC; black) and intrahepatic (IHL; red) T cells (23 biological replicates). **(c-d)** Example gating, histograms, and summary data for LC3 staining of **(c)** CD161<sup>-</sup>, CD161<sup>mid</sup>, and mucosal associated invariant T cells (MAITs, CD161<sup>hi</sup> V $\alpha$ 7.2<sup>+</sup>; 11-14 biological replicates) and **(d)** CD19<sup>+</sup> (B cells) and CD56<sup>+</sup>

(NK cells) lymphocytes (10 biological replicates). **(a, c, d)** Cells were bafA1 treated unless stated (unblocked data in **Figure S1**). **(b, d)** Wilcoxon paired t-test. **(c)** For pairwise multiple comparisons (within PBMC/IHL comparisons) Friedman test (ANOVA) with Dunn's post hoc test. For multiple unpaired comparisons (between PBMC and IHL for a given subset) Kruskal-Wallis (ANOVA) with Dunn's post hoc test. **(b, c, d)** bars at mean. \*P < 0.05; \*\*P < 0.005; \*\*\*\*P < 0.0001.

**Figure 2. High autophagy level of intrahepatic T cells is not a result of a difference in differentiation status or recent proliferation;** **(a)** Example plot of CD45RA vs. CCR7 staining (CD8<sup>+</sup> T cells) from a PBMC or IHL sample and summary data for LC3 staining of CD8<sup>+</sup> T cell memory subsets (PBMC, IHL, 9 and 15 biological replicates; Box whisker, Tukey). **(b)** Comparison of LC3 staining of CD8<sup>+</sup> T cell memory subsets between paired PBMC and IHL samples (9 biological replicates; Box whisker, Tukey, outliers shown as dots). **(c)** *Ex vivo* CD8<sup>+</sup> T cell Ki67 expression. **(d)** Example plots (CD8<sup>+</sup> T cells, PBMC) and **(e)** summary data for LC3 staining on Ki67<sup>-</sup> and Ki67<sup>+</sup> CD8<sup>+</sup> T cells in PBMC and IHL *ex vivo* (10 biological replicates) or after anti-CD3/CD28 stimulation (overnight, 0.5 µg/ml each; 3 biological replicates) in PBMC. **(f)** Histograms showing the dilution of CTV, LC3 staining, and co-staining of LC3 and CTV on CD8<sup>+</sup> T cells after five days stimulation with anti-CD3/CD28 (Red), compared to without stimulation (grey), or without CTV staining (black; two representative biological replicates of 5, PBMC). **(a-f)** Cells bafA1 treated. **(a, b)** Friedman test (ANOVA) with Dunn's post hoc test for pairwise multiple comparisons. **(c, e)** Mann-Whitney t-test. \*P < 0.05; \*\*P < 0.005; \*\*\*P < 0.001.

**Figure 3. Autophagy levels are highest in T cells that reside long-term in the liver:** (a) tSNE was applied to flow cytometry data (single cell expression values from total live CD45<sup>+</sup> singlet lymphocytes for: CD3, CD4, CD8 $\alpha$ , CD19, CD103, CD69, pan- $\gamma\delta$  TCR, pan- $\alpha\beta$  TCR, CD161, CD56, LC3) to generate a two-dimensional map of lymphocytes from paired PBMC (left) and IHL (middle) samples from two individuals. Cells are coloured by lymphocyte subset (left; example gating **Figure S1a**), and by intensity of LC3 staining for PBMC and IHL combined (middle). CD8<sup>+</sup> T<sub>RM</sub> (pan- $\alpha\beta$  TCR<sup>+</sup>CD3<sup>+</sup>CD8<sup>+</sup>CD69<sup>+</sup>CD103<sup>+/-</sup>) and MAITs (CD3<sup>+</sup>CD161<sup>hi</sup>TCR-V $\alpha$ 7.2<sup>+</sup>; right) are plotted (right). (b) Representative plots (c) and cumulative data of LC3 staining on liver-resident (CD69<sup>+</sup>CD103<sup>-</sup> [black] and CD69<sup>+</sup>CD103<sup>+</sup> [red] subsets) and non-resident liver infiltrating T cells (CD69<sup>-</sup>CD103<sup>-</sup> [grey]) in the human liver or CD69<sup>-</sup>CD103<sup>-</sup> T cells in the blood (white). Bars at geometric mean (see also **Figure S2**; PBMC, IHL 21 and 38 biological replicates). (d) Example images of single liver-resident (CD69<sup>+</sup>CD103<sup>+</sup>) or recirculating (CD69<sup>-</sup>CD103<sup>-</sup>) CD8<sup>+</sup> T cells from a human perfusate sample by ImageStream (See also **Figure S3**; representative of 3 biological replicates). L/Dead, fixable live dead. (e) Mean intensity of LC3 staining of T<sub>RM</sub> and recirculating intrahepatic CD8<sup>+</sup> T cells by ImageStream. (f) The percentage of T<sub>RM</sub> and recirculating intrahepatic CD8<sup>+</sup> T cells that contained 2 or more LC3 puncta by ImageStream. (g) Representative *ex vivo* dextramer staining, histograms of LC3 staining, and summary data for LC3 staining of HBV-specific (blue; see methods for panel of HBV dextramers targeting HBV core, surface, and polymerase), CMV-specific (black; pp65485-504 HLA-A\*02, NLVPMVATV) and total CD8<sup>+</sup> T cells (white), in PBMC from patients chronically infected with HBV (**Table S1**; 10 biological replicates). (e-f) Representative examples from one of two technical replicates. (a-g) Cells bafA1 treated (unblocked data in **Figure S3**). (c) Kruskal-Wallis (ANOVA) with Dunn's post hoc test for multiple unpaired

comparisons. **(c, e, f)** Friedman test (ANOVA) with Dunn's post hoc test multiple paired comparisons. **(g)** Wilcoxon t-test. \* $P < 0.05$ ; \*\* $P < 0.005$ ; \*\*\*\* $P < 0.0001$ .

**Figure 4. Enhanced autophagy levels are linked to effector function and mitochondrial fitness in human T cells;** **(a)** Example plots of IFN $\gamma$ , LC3, granzyme B (GzB) and perforin (perf; gated on CD8 $^{+}$  T cells), and histograms of LC3 staining for PBMC *ex vivo* or after anti-CD3/CD28 stimulation (3 days; See also **Figure S3**). **(b)** LC3 staining of CD8 $^{+}$  T cells from unstimulated PBMC (IFN $\gamma^{-}$ ), and IFN $\gamma^{-}$  and IFN $\gamma^{+}$  CD8 $^{+}$  T cells after anti-CD3/CD28 stimulation (3 days; 8 biological replicates). **(c-d)** LC3 staining on GzB and perf expressing CD8 $^{+}$  T cells **(c)** *ex vivo* and **(d)** after anti-CD3/CD28 stimulation (3 days; 8 biological replicates; Box whisker, Tukey). **(e)** Example mitochondrial staining of CD8 $^{+}$  T cells in blood (PBMC; black) and liver (IHL; red) and summary data for the *ex vivo* percentage of total CD8 $^{+}$  T cells with depolarised mitochondria (mitoTracker deep red [MtDR] $^{lo}$ ; See also **Figure S4**; PBMC 10, IHL 15 biological replicates). **(f)** *ex vivo* percentage of CD8 $^{+}$  T $_{RM}$  subsets in the liver with depolarised mitochondria (14 biological replicates; Box whisker, Tukey, outliers shown as dots). **(g)** The percentage of total CD8 $^{+}$  T cells or CD8 $^{+}$  T $_{RM}$  subsets with depolarised mitochondria after overnight culture of IHL with DMSO (untreated), MRT68921 dihydrochloride (10  $\mu$ M), bafA1 (0.1  $\mu$ M), or Reagent A (chloroquine diphosphate, 1:1000, FlowCelect LC3 kit; 13-15 biological replicates). **(a-d)** Cells bafA1 treated. **(b, e, g)** Bars at mean. **(b, c, d, f)** Friedman test (ANOVA) with Dunn's post hoc test for pairwise multiple comparisons. **(g)** Kuskal-Wallis test with Dunn's post hoc test for unpaired multiple comparisons. **(e)** Mann-Whitney unpaired t-test for total CD8 $^{+}$  PBMC vs. IHL. **(g)** Wilcoxon

paired t-test for untreated vs. MRT68921 treated. (e, g) Bars at mean. \*P < 0.05; \*\*P < 0.005; \*\*\*P < 0.001; \*\*\*\*P < 0.0001.

**Figure 5. *De novo* induced T<sub>RM</sub> have a high level of autophagy and T<sub>RM</sub> induction is abrogated when autophagy is inhibited;** (a) LC3 staining of CD8<sup>+</sup> T cells after 6 day culture of PBMC with the following cytokines: recombinant human TGFβ (rhTGFβ, 50 ng/ml) at day 0, recombinant human IL15 (rhIL15, 50 ng/ml) at day 0, sequential rhIL15 at day 0 then rhTGFβ at day 3 (bars at median; 9-24 biological replicates). (b) LC3 staining of CD8<sup>+</sup> T cells after 3 day culture of PBMC or isolated CD8<sup>+</sup> T cells with rhIL15 alone or with anti-IL15 blocking antibody (3-7 biological replicates). (c) LC3 staining of CD8<sup>+</sup> T cells after 3 days co-culture of PBMC with isolated primary human hepatic stellate cells (pHSCs; 7 biological replicates) and in the presence of IL15 blocking with rhIL15Rα-Fc chimera (0.01μg/ml; 4 biological replicates). Box-whisker, Tukey, outliers shown as dots. (d) Example plots of T<sub>RM</sub> induction and histograms of LC3 staining after 6 days culture with sequential rhIL15 at day 0 then rhTGFβ at day 3 with and without autophagy inhibitors: MRT68921 dihydrochloride (1 μM), and 3-MA (3-Methyladenine, 0.5 mM). (e) LC3 staining and (f) magnitude of the induced CD69<sup>+</sup>CD103<sup>+</sup> T<sub>RM</sub> population as a percentage of CD8<sup>+</sup> T cells after 6 days culture with and without autophagy inhibitors (10-32 biological replicates). (g) Phenotypic changes in total CD8<sup>+</sup> T cells post-stimulation with anti-CD3/CD28 (3 days) with and without the autophagy inhibitors (6 biological replicates). (a, b, d-g) Cells bafA1 treated. (a, e, f) Kruskal-Wallis (ANOVA) with Dunn's post hoc test for multiple unpaired comparisons. (b, c) Friedman test (ANOVA) with Dunn's post hoc test for pairwise multiple comparisons. (g) One-way ANOVA with Holm-sidak post hoc test multiple paired

comparisons unstimulated vs. other treatments.\*P < 0.05; \*\*P < 0.005; \*\*\*P < 0.001; \*\*\*\*P < 0.0001.

## **STAR METHODS**

### **LEAD CONTACT AND MATERIALS AVAILABILITY**

Further information and requests for resources and reagents should be directed to and will be fulfilled by the Lead Contact, Leo Swadling ([l.swadling@ucl.ac.uk](mailto:l.swadling@ucl.ac.uk)). This study did not generate any new unique reagents.

### **EXPERIMENTAL MODEL AND SUBJECT DETAILS**

#### **Subjects and recruitment**

This study was approved by the local ethical boards of London-Brent (Research Ethics Committee reference number 16/LO/1699) and Brighton and Sussex (Research Ethics Committee reference number 11/LO/0421). Each participant gave written informed consent before inclusion. All storage of samples obtained complied with the requirement of the Data Protection Act 1998 and the Human Tissue Act 2004, issued by the UK parliament. The influence of gender of human subjects used in this study was only considered for data in **Figure 4g**, where significant inter-individual variation was observed. No influence of gender was seen (Mann-Whitney t-test female vs. male  $p = 0.57$  not significant). The gender of participants was not routinely collected with anonymised clinical data for healthy volunteers and tissue donors.

#### **Sample collection**



Resected liver tissue from the healthy margins of tumor resections (colorectal metastases, adenocarcinoma, cholangiocarcinoma, hepatocellular carcinoma) and paired blood samples were obtained through the Tissue Access for Patient Benefit (TAPb) scheme at The Royal Free Hospital (approved by the University College London–Royal Free Hospital BioBank Ethical Review Committee; Research Ethics Committee reference number 11/WA/0077). Perfusion liquid was obtained from healthy livers prior to solid-organ transplantation (Research Ethics Committee reference 11/H0720/4).

For comparison, peripheral blood samples from healthy control individuals were included within the study (approved by the South East Coast Research Ethics Committee; Research Ethics Committee reference number 11/LO/0421; IRAS project number, 43993). All healthy control participants used within the study were anti-HBV, anti-hepatitis C, and anti-HIV antibody negative. Sample sizes are given in the legends for all experiments where individual data points are not shown.

## **METHOD DETAILS**

### **PBMC and IHL isolation**

PBMC were isolated by density centrifugation. Heparinised blood was layered on Ficoll-Hypaque Plus (GE Healthcare) or Pancoll (Pan Biotech) and was centrifuge for 20 minutes (mins) 800 g with slow acceleration and without brake. IHL were isolated from perfusion liquid by first concentrating the cells by centrifugation (300 g 10 mins) and resuspension in RPMI 1640 (Thermo Fisher Scientific). The concentrated cell suspension was then layered on Ficoll-Hypaque Plus as above.

Explanted liver tissue sections were cut into small pieces using scissors and were incubated for 30 min in 0.01% collagenase IV (Thermo Fisher Scientific) and 0.001% DNase I (Roche) at 37 °C in a humidified atmosphere with 5% CO<sub>2</sub>. After enzymatic digestion, mechanical digestion was performed using a GentleMACS (Miltenyi Biotec). After full digestion, debris was removed by passing single cell suspension through 70 µM cell strainers (BD biosciences). Parenchymal cells were removed by centrifugation (400 g) on a 30% Percoll gradient (GE Healthcare). Finally, IHL were isolated by density centrifugation using Ficoll-Hypaque Plus as above.

All experiments using paired IHL and PBMC were performed *ex vivo* on freshly isolated cells. For ImageStream experiments frozen IHL isolated from perfusion fluid were used. All experiments using PBMC from healthy controls used frozen PBMC. PBMC and IHL were frozen in 10% DMSO (Sigma-Aldrich) in Isopropanol containers (-1°C/minute) at 5-20 x 10<sup>6</sup> PBMC/ml in cryovials. Thawing was performed by gentle agitation at 37°C with rapid dilution in RPMI containing 10% fetal bovine serum (FBS; Sigma-Aldrich) and 0.001% DNase I. RPMI 1640 + 10% FBS, 100 U/ml penicillin/streptomycin was used for T cell culture media (R10).

### **Flow cytometry – Surface, intracellular, intranuclear, and cytokine staining**

For multiparametric flow cytometry cells were plated in 96-well round-bottomed plates (200,000-1,000,000) and washed once in PBS (Phosphate buffered saline; Thermo Fisher Scientific) and stained with a fixable live/Dead dye (Thermo Fisher Scientific) for 20 mins at 4 °C in PBS. Cells were washed again in PBS, and incubated with saturating concentrations of surface monoclonal antibodies (mAbs) diluted in 50% Brilliant violet buffer (BD biosciences) and 50% PBS for 30 min at 4°C unless stated. For surface marker assessment alone cells were then fixed with 1% formaldehyde (Sigma-Aldrich) in PBS for 20 mins 4°C and washed twice in

PBS before being analysed on a flow cytometer.

For intracellular and intranuclear staining, after surface Ab staining cells were resuspended in fix/perm buffer (Foxp3 / Transcription Factor staining buffer kit, fix perm concentrate diluted 1:3 in fix/perm diluent) for 45-60 mins at 4 °C. Cells were then washed in 1x perm buffer (10x perm buffer Foxp3 / Transcription Factor staining buffer kit diluted to 1X in ddH<sub>2</sub>O) and saturating concentrations of antibodies against intranuclear targets were stained in 1X perm buffer for 30-45 mins 4 °C. Cells were washed twice in PBS then analysed by flow cytometry. For intracellular cytokine staining PBMC 1 hour after stimulation 1 µg/ml brefeldin A (Sigma-Aldrich) was added and PBMC were incubated for 16 hours at 37 °C in a humidified atmosphere with 5% CO<sub>2</sub>. For stimulation by CD3-crosslinking with co-stimulation anti-CD3 and anti-CD28 (eBioscience) antibodies were diluted to 0.5 µg/ml in PBS and incubated on Nunclon delta surface 96-well round-bottom plates (Thermo Fisher Scientific) for 1 hour. Plates were washed three times with PBS and then cells were added in culture media.

All samples were acquired in PBS on LSRII or Fortessa X20 flow cytometers (BD biosciences) and analysed using FlowJo (version 10.4.1 for mac, Tree Star). Single stain controls were prepared with cells where possible or anti-mouse IgG beads (BD biosciences) and Arc-Amine reactive beads (Thermo Fisher Scientific).

### **Flow cytometry based LC3-I quantification**

To quantify the number of autophagosome *ex vivo*, or the accumulation of autophagosomes (after inhibiting autophagosome degradation) as proxies for the level of autophagy or autophagic flux respectively, the FlowCollect Autophagy LC3 Antibody-based Assay Kit (Merck Millipore, now Luminex) was used (Eng et al. 2010). A proprietary permeabilisation buffer (Autophagy reagent

B) is used to selectively extract non-autophagosome associated cytosolic LC3-I; therefore, when the anti-LC3 antibody is added only the lipidated form LC3-II incorporated within autophagosomes remains and is stained. The fluorescence of the anti-LC3-FITC antibody can then be used to quantify autophagosomes.

For *ex vivo* assessment of autophagy levels autophagosomes were stained by flow cytometry using a fluorescently labelled anti-LC3 antibody (clone 4E12). PBMC or IHL were washed, stained for live/dead marker and then surface markers as above. Cells were then centrifuged at 300 g 4 mins 4 °C and resuspended in 50 µl autophagy reagent B permeabilisation buffer (Diluted 1:10 in ddH2O) per well and immediately centrifuged 300 g 4 mins 4 °C and resuspended in anti-LC3-FITC (1:20 50ul/well) diluted in assay buffer (assay buffer concentrate is diluted 1:5 in ddH2O) and incubated at 4 °C for 30 mins. Cells were then washed in PBS, resuspended in 1% formaldehyde to fix for 20 mins at 4 °C, washed in PBS, and run on a flow cytometer.

The geometric mean fluorescence intensity (geoMFI) of LC3 *ex vivo* without addition of bafilomycin A1 (“unblocked”) was used to define the basal autophagy level. To measure the accumulation of autophagosomes over time 0.1 µM bafilomycin A1 (“blocked”; Sigma-Aldrich; diluted in DMSO; (Klionsky et al. 2016; Clarke et al. 2018; Puleston et al. 2014), was added to cell cultures overnight (**Figure 1, Figure 2 [excluding panel f], Figure 3, Figure 5e-f, Figure S1c-d**) for paired IHL and PBMC samples, or for 3 hours for all other experiments (**Figure 2f, Figure 4, Figure 5; Figure 5g-h are unblocked**)(See **Figure S1b,c, S2, S3c and S3c** for comparisons of unblocked and bafilomycin A1 blocked staining). The ratio of geoMFI LC3 (flux) for blocked vs. unblocked was calculated as follows: (+bafA1 blocked geoMFI LC3 -

unblocked geoMFI LC3) / unblocked geoMFI LC3.

When LC3 was co-stained with intracellular or intranuclear markers (**Figure 2c-e, Figure 4a-d**) PBMC were fixed with fix/perm buffer (Foxp3/Transcription Factor staining buffer kit) as above and anti-LC3 was added to the intracellular antibody cocktail in perm buffer (Foxp3 / Transcription Factor staining buffer kit). Non-autophagosome associated cytosolic LC3-I is not selectively extracted using reagent B in this protocol, therefore, a common background of LC3-I is also labelled. PBMC samples were stained in parallel using the FlowCelect Autophagy LC3 Antibody-based Assay Kit as above or the BD Foxp3/Transcription Factor staining buffer kit (**Figure S3e-f**). A strong positive correlation between the two staining conditions confirmed that the samples with higher rates of autophagy by the standard protocol also had a higher level of LC3 staining when stained with the intracellular protocol, and that the LC3-I background level was consistent across samples and treatments. Samples stained by the intracellular protocol or FlowCelect Kit were measured on separate Flow Cytometers with different panels however, so direct comparisons of the MFI magnitude cannot be made.

Intracellular staining of p62 (sequestosome 1; SQSTM1; Abcam) was performed as described in (Clarke et al. 2015). IHL were incubated overnight with or without bafA1 (0.1  $\mu$ M). The following day after fixable live/dead stain and surface Ab staining as above cells were fixed in 1 % formaldehyde for 20 mins at 4 °C. Cells were then permeabilised in 1x perm buffer (10x perm buffer Foxp3 / Transcription Factor staining buffer kit diluted to 1X in ddH<sub>2</sub>O) for 20 mins at 4 °C and then saturating concentration of anti-p62-alexa647 was added in 1X perm buffer for 30 mins 4 °C. Cells were washed in 1x perm buffer and then PBS before acquiring. The ratio of geoMFI p62 (sequestosome 1; SQSTM1; abcam) (flux) for blocked vs. unblocked was calculated as follows: (+bafA1 blocked geoMFI p62 - unblocked geoMFI p62) / unblocked geoMFI p62.

## **Flow cytometry based autophagosome quantification using Cyto-ID**

Cyto-ID is a proprietary dye that includes titratable moieties specific for staining autophagic vesicles (Enzo Lifesciences). To measure autophagy in T cells using the Cyto-ID autophagy detection kit (ENZ-51031-0050) PBMC and IHL were thawed (as above) and rested overnight in R10 culture media in 96-well plates at  $0.5 \times 10^6$  PBMC per well at 37 °C in a humidified atmosphere with 5% CO<sub>2</sub>. Plates were centrifuged at 300 g 4 mins RT and cell pellets were resuspended in pre-warmed (37°C) RPMI without phenol red (Thermo Fisher Scientific) containing 5% FBS, 100 U/ml penicillin/streptomycin and Cyto-ID dye diluted 1:4000. Cells were incubated with Cyto-ID at 37 °C in a humidified atmosphere with 5% CO<sub>2</sub> for 30 mins before being washed with the Cyto-ID kit assay buffer diluted to 1X in sterile distilled H<sub>2</sub>O. Cells were then stained with fixable live/dead, stained with surface antibodies, fixed with 1% formaldehyde, and analysed by flow cytometry as above for the surface staining protocol.

## **Autophagy inhibitors**

MRT68921 dihydrochloride (Sigma-Aldrich; used at 1 or 10 µM for 6 day or overnight cultures respectively) is an autophagy specific ULK1 and ULK2 kinases inhibitor ((Klionsky et al. 2016; Petherick et al. 2015). 3-Methyladenine (3-MA; Sigma-Aldrich; 0.5 mM) is a type I and III Phosphatidylinositol 3-kinases (PI-3K) inhibitor (Wu et al. 2010).

## **MitoTracker staining**

Freshly isolated IHL and PBMC were stained *ex vivo* with cell permeable mitochondrial dyes by adding them directly to culture media. MitoTracker Deep Red FM and MitoTracker Green FM (Thermo Fisher Scientific) were added to a final concentration of 12.5 nM and 25 nM in the well

respectively and were stained for 20 mins at 37 °C in a humidified atmosphere with 5% CO<sub>2</sub>. Cells were then washed in PBS and stained with fixable live/dead and surface antibodies as above. Cells were left unfixed for flow cytometric analysis. For overnight inhibition of autophagy (**Figure 4g-h**) bafilomycin A1 (0.1 µM), Reagent A (Chloroquine diphosphate, FlowCollect Autophagy LC3 Antibody-based Assay Kit), MRT68921 dihydrochloride, or DMSO vehicle were added to R10 culture media and cells were stained for MitoTrackers as above after ~16 hours culture.

For inhibition of efflux pumps verapamil (Sigma-Aldrich; 50 µM) and cyclosporin A (Sigma-Aldrich; 50 µM) were added directly to culture media with the mitoTracker dyes and incubated for 20 mins at 37 °C in a humidified atmosphere with 5% CO<sub>2</sub> and mitoTracker staining was as above.

## **ImageStream**

ImageStream has been used extensively to directly image intracellular autophagosomes using fluorescently labelled anti-LC3 antibodies (Clarke et al. 2018; Klionsky et al. 2016; Phadwal et al. 2012; Sanderson & Simon 2017; Puleston et al. 2014).

IHL and PBMC were thawed as above and were cultured overnight (16 hours) in R10 culture media supplemented with 0.1 µM bafilomycin A1. Cells were washed and T cells were isolated using negative magnetic bead selection (panT cell isolation kit, Miltenyi Biotec) according to the manufacturer's instructions. T cells were collected on ice, counted, stained as above for surface markers and intracellular LC3 and fixed with 1% formaldehyde. The following panel was used: Camera 1; Ch1 Bright field, Ch2 LC3-FITC, Ch3 CD4-PE, Ch5 CD8-PerCp-Cy5.5, Ch6 SSC. Camera 2 Ch8 CD69-V500, Ch10 CD103-BV605, Ch12 Near Infrared-fixable live/dead.

Amnis ImageStream<sup>X</sup> imaging flow cytometer (MERK-Millipore) fitted with a 60× microscope objective was used for cell imaging. Raw image files were acquired using INSPIRE software. After acquisition, a compensation matrix was applied to the data to correct for spectral overlap. Data analysis was done using IDEAS software, displaying cells using gradient RMS for the bright field channel to exclude out-of-focus cells and a combined area to aspect ratio dot plot ensured gating on single-cell events (see **Figure S3** for gating and staining controls).

### **T cell proliferation assay**

Frozen PBMC were thawed at 37 °C as described above and washed twice with sterile PBS. PBMC were resuspended in 1 ml R10 culture media ( $2-10 \times 10^6$  PBMC) and 0.5 µl of 5 mM stock CellTrace violet (Thermo Fisher Scientific) was added per sample with mixing. PBMC were stained in the dark for 10 mins at 37 °C in a humidified atmosphere with 5% CO<sub>2</sub>. Ten-times volume of cold R10 was added to stop the staining reaction, and cells were incubated for 5 mins on ice. Cells were washed in PBS and incubated for 5 mins at 37 °C before being transferred to a new tube and were washed again in R10. CTV stained and unstained control PBMC were plated in 48-well plates ( $0.5 \times 10^6$  PBMC in 0.5 ml R10) stimulated with plate bound anti-CD3/CD28 cross-linking antibodies (0.5 µg/ml each added for 1 hr in PBS, washed with 3 x 1 ml PBS) for 5 days, or in uncoated wells (unstimulated control). At the end of the 5 days, PBMC were harvested from the 48-well plate and were transferred to a 96-well plate and were incubated with bafilomycin A1 for 3 hours, before being washed and stained for fixable live/dead, surface Abs, and LC3 as above.

### **MHC class I dextramer staining for the identification of antigen-specific T cells**



HBV-specific HLA-A\*02-restricted dextramers (Immudex) of the following specificities were used: core<sub>18–27</sub> (FLPSDFFPSV), envelope<sub>183–191</sub> (FLLTRILTI), envelope<sub>335–342</sub> (WLS LLVPFV), envelope<sub>338–347</sub> (LLVPFVQWFV), envelope<sub>348–357</sub> (GLSPTVWLSV), polymerase<sub>455–463</sub> (GLSRYVARL), and polymerase<sub>502–510</sub> (KLHLYSHPI). CMV specific CD8<sup>+</sup> T cell responses were tracked using an HLA-A\*02-restricted dextramers (Immudex) loaded with the pp65<sub>495–504</sub> (NLVPMVATV) peptide. PBMC were thawed, rested for 1 hour, and then incubated at 37 °C in a humidified atmosphere with 5% CO<sub>2</sub> overnight with bafilomycin A1 (0.1 μM). PBMC were washed in PBS and were stained with dextramers at room temperature (20mins) in PBS, washed twice in PBS before further mAb staining as described above. During analysis, stringent gating criteria were applied with doublet and dead cell exclusion to minimise nonspecific binding contamination. A dextramer loaded with an irrelevant peptide was stained in parallel to assess non-specific binding. Dextramer clouds of less than 50 cells were excluded from analysis.

### ***In vitro* Induction of T<sub>RM</sub> phenotype**

For *in vitro* tissue-resident T cell induction, PBMC from healthy controls were incubated at  $5 \times 10^5$  cells/well in 0.5 ml R10 culture media (supplemented with 20 IU/ml recombinant human IL2 at day 0 and day 3, Miltenyi Biotec) for 6 days with different combinations of cytokines (recombinant human TGFβ, rhTGFβ, 50 ng/ml; recombinant human IL15, rhIL15, 50 ng/ml). On day 6 PBMC were harvested from the 48-well plate, transferred to a 96-well plate and were incubated with bafilomycin A1 for 3 hours, before being washed and stained for fixable live/dead, surface Abs, and LC3 as above. Autophagy inhibitors were added throughout the culture, at day 0, day 3, and during the 3 hour incubation with bafilomycin A1.

For 3 day cultures, PBMC were plated in R10 culture media supplemented with different doses

of IL15, without IL2. On day 3 PBMC were harvested from the 48-well plate, transferred to a 96-well plate and were incubated with bafilomycin A1 for 3 hours, before being washed and stained for fixable live/dead, surface Abs, and LC3 as above.

### **Primary human hepatic stellate cell co-culture**

For extraction of primary human hepatic stellate cells (HSCs), fresh post-resection liver tissue was washed thoroughly, passed through a tissue press and digested with DNase I (0.001%) and collagenase IV (0.01%). Cellular homogenate was filtered through a 70  $\mu$ m cell strainer and centrifuged at low speed to remove remaining parenchymal cells, then at 450 g to wash the cells. The remaining cells were layered for density gradient isolation using Optiprep (Sigma-Aldrich). After isolation, HSCs were suspended in Stellate Cell Medium (ScienCell Research Laboratories), plated at a density of  $5 \times 10^4$  cells/cm in tissue culture flasks and cultured at 37 °C in a humidified atmosphere with 5% CO<sub>2</sub>. On day 2, 3 or 4, cell debris and non-adherent cells were removed by washing. When cultures reached confluence, cells were trypsinised and re-plated; cells were passaged twice before freezing.

Pre-isolated HSCs were thawed and cultured in 25 cm<sup>2</sup> tissue culture flasks in Stellate Cell Medium to approximately 90% confluence. Cells were detached with trypsin–EDTA (Thermo Fisher Scientific), re-plated in 48-well plates in Stellate Cell Media (5,000-20,000 HSCs per well) and left for 36-48 hours to adhere. Media was removed and  $5 \times 10^5$  PBMC/well were added with R10 culture media and cells were co-cultured for 3 days. rhIL15R $\alpha$ -Fc chimera (0.01 $\mu$ g/ml; R&D systems) was added to R10 culture media with PBMC prior to being plated on HSCs. On day 3 PBMC were harvested from the 48-well plate, transferred to a 96-well plate and were washed and stained for fixable live/dead, surface Abs, and LC3 as above. To confirm the

differentiation status of HSCs a sample was surface stained with  $\alpha$ -SMA and ICAM-1 at the end of the 3 days culture.

## **QUANTIFICATION AND STATISTICAL ANALYSIS**

### **t-Distributed Stochastic Neighbor Embedding (tSNE) analysis**

The dimension reduction algorithm tSNE was applied to concatenated flow cytometry data (~180,000 cells) from 2 paired IHL and PBMC samples using default parameters (iterations, 1,000; perplexity, 20; and  $\theta$ , 0.5) in FlowJo. tSNE was applied to expression data for CD3, CD4, CD8 $\alpha$ , CD19, CD103, CD69, pan- $\gamma\delta$  T cell Receptor (TCR), pan- $\alpha\beta$  TCR, CD161, CD56, and LC3 after pre-gating on single, live, CD45<sup>+</sup> lymphocytes.

### **Statistical analysis**

Statistical analyses were performed in either Prism (Graph-Pad Software, version 7.0e) or R version 3.2.4 using appropriate methods as indicated in the legends (Mann-Whitney t test; Wilcoxon Signed-rank t test; Kruskal-Wallis test [ANOVA] for unpaired non-parametric multiple comparisons, Friedman test (ANOVA) for pairwise non-parametric multiple comparisons, both with Dunn's post hoc test; Spearman's Rank Order Correlation) with significant differences marked on all figures. All tests were performed as two-tailed tests, and for all tests, significance levels were defined as \*,  $P < 0.05$ ; \*\*,  $P < 0.01$ ; \*\*\*,  $P < 0.001$ ; and \*\*\*\*,  $P < 0.0001$ .

### **Data and Code availability**

This study did not generate any unique datasets or code.

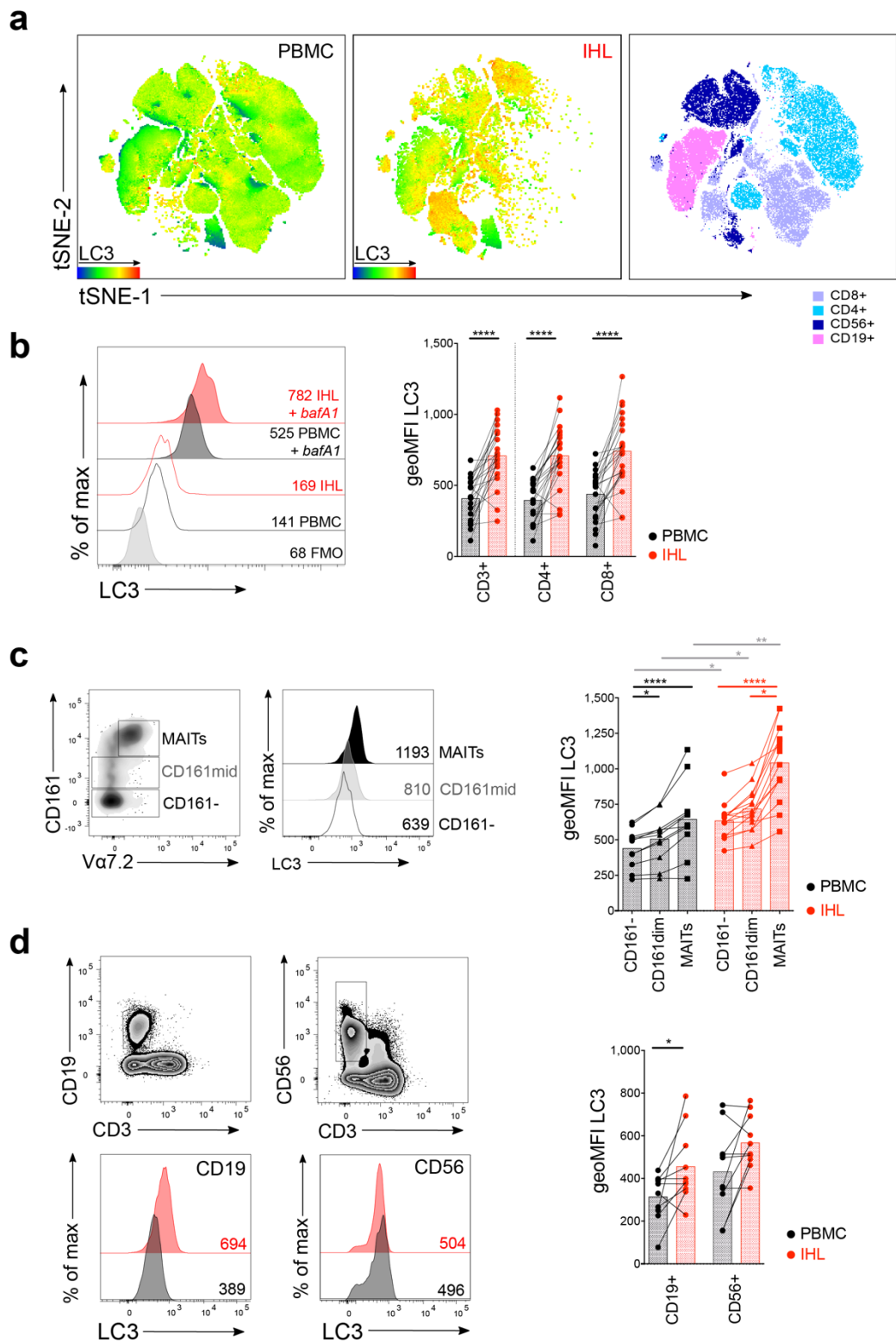


**Figure 1. Intrahepatic lymphocytes are characterised by high *ex vivo* autophagy levels; (a)**

The dimensionality reduction algorithm tSNE was applied to flow cytometry data (single cell expression values from total live CD45<sup>+</sup> singlet lymphocytes for: CD3, CD4, CD8 $\alpha$ , CD19, CD103, CD69, pan- $\gamma\delta$  T cell receptor (TCR), pan- $\alpha\beta$  TCR, CD161, CD56, LC3) to generate a two-dimensional map of lymphocytes from paired PBMC (left) and IHL (middle) samples from two individuals coloured by intensity of LC3 or by lymphocyte subset (right; example gating **Figure S1a**). **(b)** Histograms (gated on CD8<sup>+</sup>; +/- bafilomycin A1 [bafA1] treatment, 0.1  $\mu$ M; FMO for LC3)) and summary data for LC3 staining of paired peripheral (PBMC; black) and intrahepatic (IHL; red) T cells (23 biological replicates). **(c-d)** Example gating, histograms, and summary data for LC3 staining of **(c)** CD161<sup>-</sup>, CD161<sup>mid</sup>, and mucosal associated invariant T cells (MAITs, CD161<sup>hi</sup> V $\alpha$ 7.2<sup>+</sup>; 11-14 biological replicates) and **(d)** CD19<sup>+</sup> (B cells) and CD56<sup>+</sup> (NK cells) lymphocytes (10 biological replicates). **(a, c, d)** Cells were bafA1 treated unless stated (unblocked data in **Figure S1**). **(b, d)** Wilcoxon paired t-test. **(c)** For pairwise multiple comparisons (within PBMC/IHL comparisons) Friedman test (ANOVA) with Dunn's post hoc test. For multiple unpaired comparisons (between PBMC and IHL for a given subset) Kruskal-Wallis (ANOVA) with Dunn's post hoc test. **(b, c, d)** bars at mean. \*P < 0.05; \*\*P < 0.005; \*\*\*\*P < 0.0001.



samples (9 biological replicates; Box whisker, Tukey, outliers shown as dots). **(c)** *Ex vivo* CD8<sup>+</sup> T cell Ki67 expression. **(d)** Example plots (CD8<sup>+</sup> T cells, PBMC) and **(e)** summary data for LC3 staining on Ki67<sup>-</sup> and Ki67<sup>+</sup> CD8<sup>+</sup> T cells in PBMC and IHL *ex vivo* (10 biological replicates) or after anti-CD3/CD28 stimulation (overnight, 0.5 µg/ml each; 3 biological replicates) in PBMC. **(f)** Histograms showing the dilution of CTV, LC3 staining, and co-staining of LC3 and CTV on CD8<sup>+</sup> T cells after five days stimulation with anti-CD3/CD28 (Red), compared to without stimulation (grey), or without CTV staining (black; two representative biological replicates of 5, PBMC). **(a-f)** Cells bafA1 treated. **(a, b)** Friedman test (ANOVA) with Dunn's post hoc test for pairwise multiple comparisons. **(c, e)** Mann-Whitney t-test. \*P < 0.05; \*\*P < 0.005; \*\*\*P < 0.001.

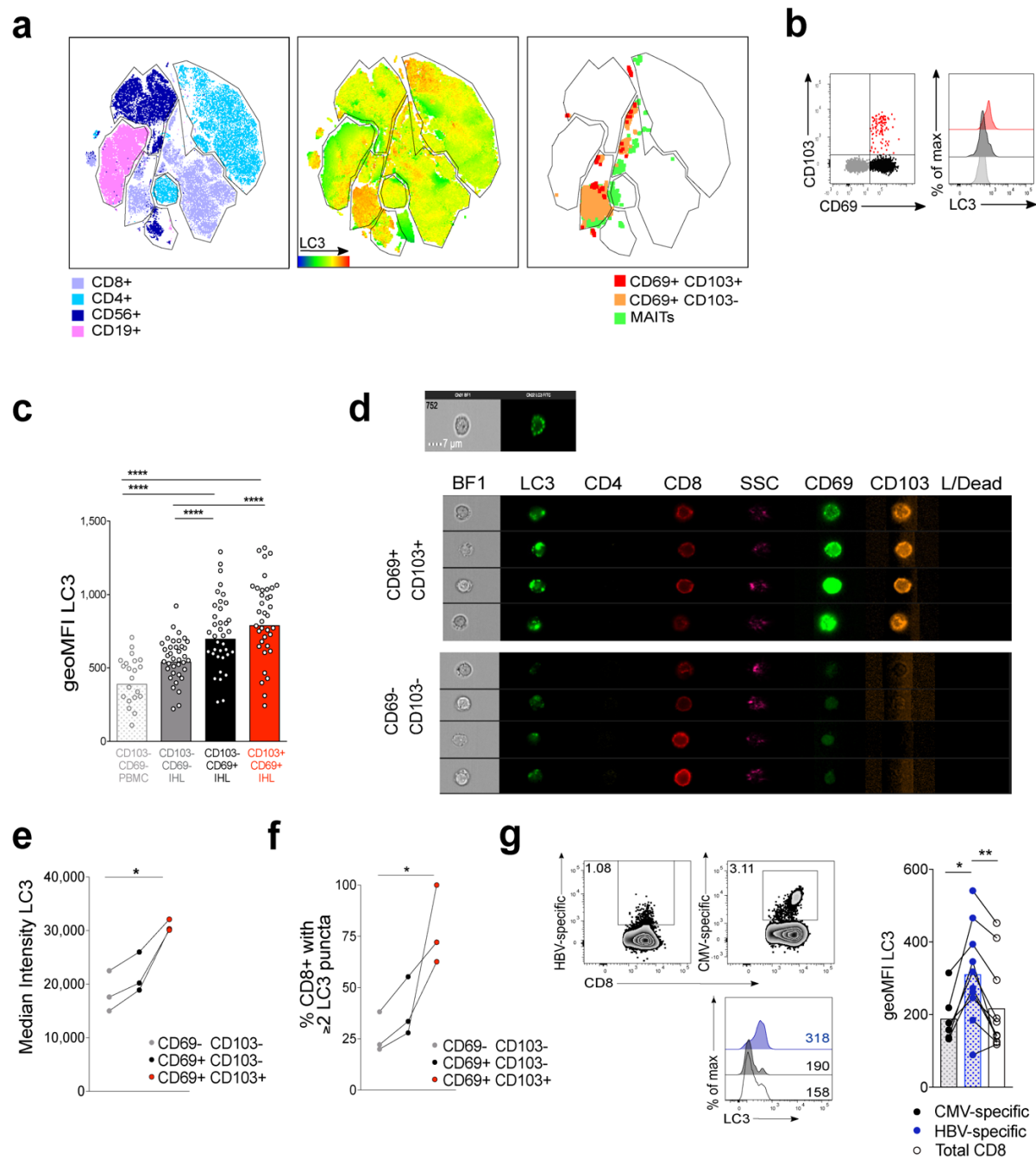


**Figure 3. Autophagy levels are highest in T cells that reside long-term in the liver:** (a) tSNE was applied to flow cytometry data (single cell expression values from total live CD45<sup>+</sup> singlet lymphocytes for: CD3, CD4, CD8 $\alpha$ , CD19, CD103, CD69, pan- $\gamma\delta$  TCR, pan- $\alpha\beta$  TCR, CD161, CD56, LC3) to generate a two-dimensional map of lymphocytes from paired PBMC (left) and



IHL (middle) samples from two individuals. Cells are coloured by lymphocyte subset (left; example gating **Figure S1a**), and by intensity of LC3 staining for PBMC and IHL combined (middle). CD8<sup>+</sup> T<sub>RM</sub> (pan- $\alpha\beta$  TCR<sup>+</sup>CD3<sup>+</sup>CD8<sup>+</sup>CD69<sup>+</sup>CD103<sup>+/-</sup>) and MAITs (CD3<sup>+</sup>CD161<sup>hi</sup>TCR-V $\alpha$ 7.2<sup>+</sup>; right) are plotted (right). **(b)** Representative plots **(c)** and cumulative data of LC3 staining on liver-resident (CD69<sup>+</sup>CD103<sup>-</sup> [black] and CD69<sup>+</sup>CD103<sup>+</sup> [red] subsets) and non-resident liver infiltrating T cells (CD69<sup>-</sup>CD103<sup>-</sup> [grey]) in the human liver or CD69<sup>-</sup>CD103<sup>-</sup> T cells in the blood (white). Bars at geometric mean (see also **Figure S2**; PBMC, IHL 21 and 38 biological replicates). **(d)** Example images of single liver-resident (CD69<sup>+</sup>CD103<sup>+</sup>) or recirculating (CD69<sup>-</sup>CD103<sup>-</sup>) CD8<sup>+</sup> T cells from a human perfusate sample by ImageStream (See also **Figure S3**; representative of 3 biological replicates). L/Dead, fixable live dead. **(e)** Mean intensity of LC3 staining of T<sub>RM</sub> and recirculating intrahepatic CD8<sup>+</sup> T cells by ImageStream. **(f)** The percentage of T<sub>RM</sub> and recirculating intrahepatic CD8<sup>+</sup> T cells that contained 2 or more LC3 puncta by ImageStream. **(g)** Representative *ex vivo* dextramer staining, histograms of LC3 staining, and summary data for LC3 staining of HBV-specific (blue; see methods for panel of HBV dextramers targeting HBV core, surface, and polymerase), CMV-specific (black; pp65485-504 HLA-A\*02, NLVPMVATV) and total CD8<sup>+</sup> T cells (white), in PBMC from patients chronically infected with HBV (**Table S1**; 10 biological replicates). **(e-f)** Representative examples from one of two technical replicates. **(a-g)** Cells bafA1 treated (unblocked data in **Figure S3**). **(c)** Kruskal-Wallis (ANOVA) with Dunn's post hoc test for multiple unpaired comparisons. **(c, e, f)** Friedman test (ANOVA) with Dunn's post hoc test multiple paired comparisons. **(g)** Wilcoxon t-test. \*P < 0.05; \*\*P < 0.005; \*\*\*\*P < 0.0001.



**Figure 4. Enhanced autophagy levels are linked to effector function and mitochondrial fitness in human T cells; (a)** Example plots of IFN $\gamma$ , LC3, granzyme B (GzB) and perforin (perf; gated on CD8 $^{+}$  T cells), and histograms of LC3 staining for PBMC *ex vivo* or after anti-CD3/CD28 stimulation (3 days; See also **Figure S3**). **(b)** LC3 staining of CD8 $^{+}$  T cells from unstimulated PBMC (IFN $\gamma^{-}$ ), and IFN $\gamma^{-}$  and IFN $\gamma^{+}$  CD8 $^{+}$  T cells after anti-CD3/CD28 stimulation (3 days; 8 biological replicates). **(c-d)** LC3 staining on GzB and perf expressing CD8 $^{+}$  T cells **(c)** *ex vivo* and **(d)** after anti-CD3/CD28 stimulation (3 days; 8 biological replicates; Box whisker, Tukey). **(e)** Example mitochondrial staining of CD8 $^{+}$  T cells in blood (PBMC; black) and liver (IHL; red) and summary data for the *ex vivo* percentage of total CD8 $^{+}$  T cells with depolarised mitochondria (mitoTracker deep red [MtDR] $^{lo}$ ; See also **Figure S4**; PBMC 10, IHL 15 biological replicates). **(f)** *ex vivo* percentage of CD8 $^{+}$  T $_{RM}$  subsets in the liver with depolarised mitochondria (14 biological replicates; Box whisker, Tukey, outliers shown as dots). **(g)** The percentage of total CD8 $^{+}$  T cells or CD8 $^{+}$  T $_{RM}$  subsets with depolarised mitochondria after overnight culture of IHL with DMSO (untreated), MRT68921 dihydrochloride (10  $\mu$ M), bafA1 (0.1  $\mu$ M), or Reagent A (chloroquine diphosphate, 1:1000, FlowCellelect LC3 kit; 13-15 biological replicates). **(a-d)** Cells bafA1 treated. **(b, e, g)** Bars at mean. **(b, c, d, f)** Friedman test (ANOVA) with Dunn's post hoc test for pairwise multiple comparisons. **(g)** Kuskal-Wallis test with Dunn's post hoc test for unpaired multiple comparisons. **(e)** Mann-Whitney unpaired t-test for total CD8 $^{+}$  PBMC vs. IHL. **(g)** Wilcoxon paired t-test for untreated vs. MRT68921 treated. **(e, g)** Bars at mean. \*P < 0.05; \*\*P < 0.005; \*\*\*P < 0.001; \*\*\*\*P < 0.0001.

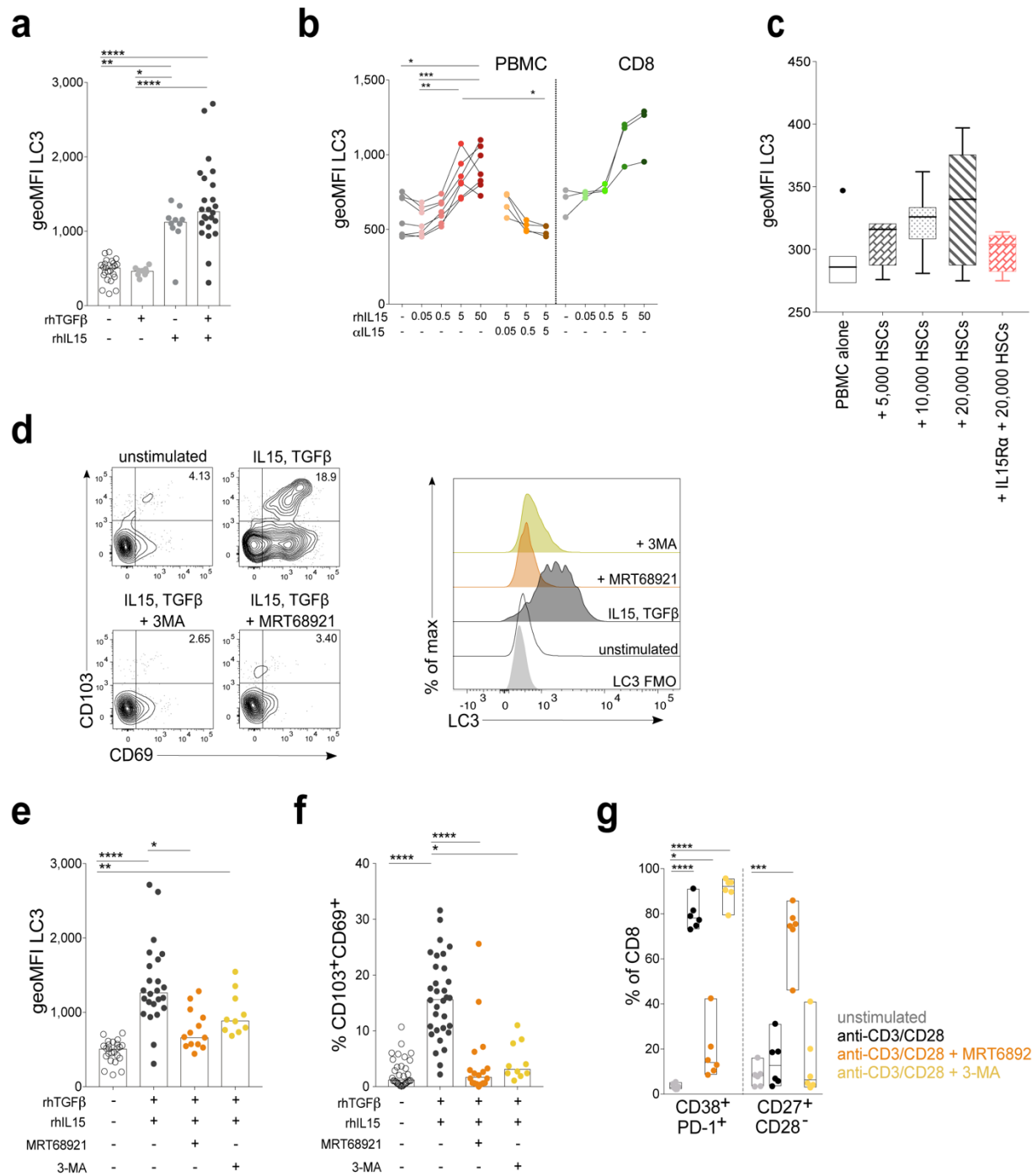


**Figure 5. *De novo* induced T<sub>RM</sub> have a high level of autophagy and T<sub>RM</sub> induction is abrogated when autophagy is inhibited; (a)** LC3 staining of CD8<sup>+</sup> T cells after 6 day culture of PBMC with the following cytokines: recombinant human TGFβ (rhTGFβ, 50 ng/ml) at day 0,

recombinant human IL15 (rhIL15, 50 ng/ml) at day 0, sequential rhIL15 at day 0 then rhTGF $\beta$  at day 3 (bars at median; 9-24 biological replicates). **(b)** LC3 staining of CD8<sup>+</sup> T cells after 3 day culture of PBMC or isolated CD8<sup>+</sup> T cells with rhIL15 alone or with anti-IL15 blocking antibody (3-7 biological replicates). **(c)** LC3 staining of CD8<sup>+</sup> T cells after 3 days co-culture of PBMC with isolated primary human hepatic stellate cells (pHSCs; 7 biological replicates) and in the presence of IL15 blocking with rhIL15R $\alpha$ -Fc chimera (0.01  $\mu$ g/ml; 4 biological replicates). Box-whisker, Tukey, outliers shown as dots. **(d)** Example plots of T<sub>RM</sub> induction and histograms of LC3 staining after 6 days culture with sequential rhIL15 at day 0 then rhTGF $\beta$  at day 3 with and without autophagy inhibitors: MRT68921 dihydrochloride (1  $\mu$ M), and 3-MA (3-Methyladenine, 0.5 mM). **(e)** LC3 staining and **(f)** magnitude of the induced CD69<sup>+</sup>CD103<sup>+</sup> T<sub>RM</sub> population as a percentage of CD8<sup>+</sup> T cells after 6 days culture with and without autophagy inhibitors (10-32 biological replicates). **(g)** Phenotypic changes in total CD8<sup>+</sup> T cells post-stimulation with anti-CD3/CD28 (3 days) with and without the autophagy inhibitors (6 biological replicates). **(a, b, d-g)** Cells bafA1 treated. **(a, e, f)** Kruskal-Wallis (ANOVA) with Dunn's post hoc test for multiple unpaired comparisons. **(b, c)** Friedman test (ANOVA) with Dunn's post hoc test for pairwise multiple comparisons. **(g)** One-way ANOVA with Holm-sidak post hoc test multiple paired comparisons unstimulated vs. other treatments.\*P < 0.05; \*\*P < 0.005; \*\*\*P < 0.001; \*\*\*\*P < 0.0001.

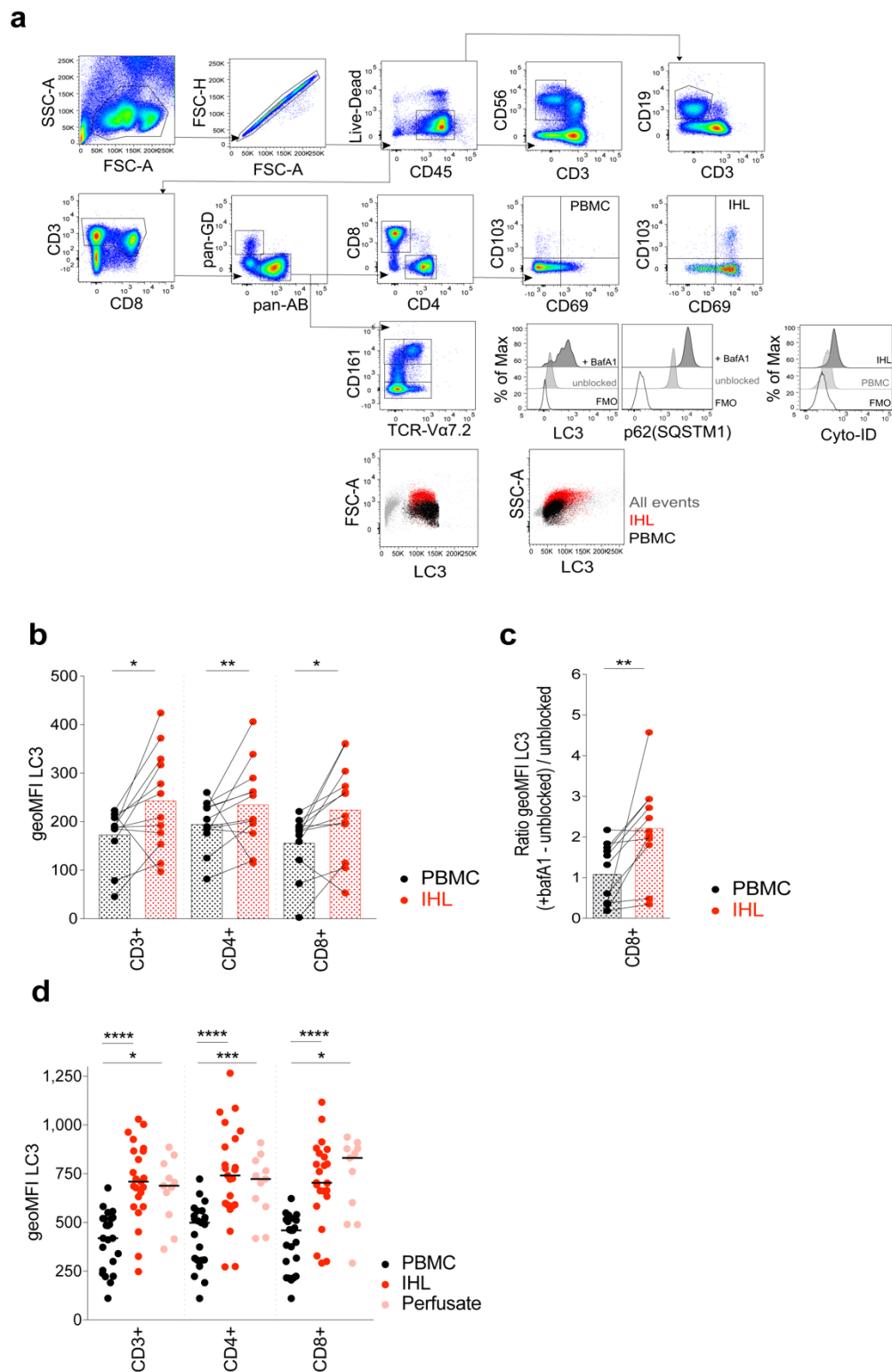


**Figure S1. Sequential gating strategy for lymphocyte subsets and LC3 liver staining controls; Related to Figure 1; (a) Sequential gating strategy to identify: lymphocytes (SSC-A**

vs. FSC-A)/single cells (FSC-H vs. FSC-A)/live CD45<sup>+</sup> lymphocytes (Fixable live/dead<sup>-</sup> CD45<sup>+</sup>)/NK cells (CD56<sup>+</sup> CD3<sup>-</sup>), B cells (CD19<sup>+</sup> CD3<sup>-</sup>), T cells (CD3<sup>+</sup>)/pan- $\gamma\delta$  and pan- $\alpha\beta$  T cells (pan- $\gamma\delta$  TCR vs. pan- $\alpha\beta$  TCR)/MAITs (CD161<sup>hi</sup> TCR-V $\alpha$  7.2<sup>+</sup>) and CD161mids (CD161<sup>mid</sup> TCR-V $\alpha$  7.2<sup>-</sup>), CD4<sup>+</sup> and CD8<sup>+</sup> T cells (CD4 vs. CD8)/tissue-resident T cells (CD103 vs. CD69; shown for PBMC and IHL). Also shown are example histograms of LC3 and p62 (Sequestosome-1, SQSTM1) staining of IHL treated with bafilomycin A1 (bafA1) overnight or untreated (DMSO vehicle), and Cyto-ID staining of IHL and PBMC, all gated on CD8<sup>+</sup> T cells with example fluorescence minus one stains (FMO). FSC-A vs. LC3 and SSC-A vs. LC3 plots are shown for all events (grey), CD3<sup>+</sup> T cells in PBMC (black) and CD3<sup>+</sup> T cells in IHL (red), showing a higher LC3 staining for cells of equivalent size and granularity in IHL samples relative to PBMC samples. **(b)** Summary data of the geoMFI of LC3 on CD3<sup>+</sup>, CD4<sup>+</sup>, and CD8<sup>+</sup> T cells in paired PBMC and IHL samples *ex vivo* without bafA1 treatment (unblocked; bars at mean; 12 biological replicates). **(c)** The ratio of geoMFI LC3 between accumulated (blocked; + bafA1) and basal (unblocked) samples for CD8<sup>+</sup> T cells from paired PBMC and IHL samples calculated as follows: (geoMFI LC3 with bafA1 – unblocked geoMFI LC3) / unblocked geoMFI LC3; 11 biological replicates). **(d)** Summary data for CD3<sup>+</sup>, CD4<sup>+</sup>, and CD8<sup>+</sup> T cells in perfusion fluid (perfusate) and paired PBMC and IHL samples *ex vivo*. bafA1 treated (23 biological replicates for paired blood and IHL, 11 biological replicates for perfusates). **(b, c)** Wilcoxon paired t-tests. **(d)** Kruskal-Wallis (ANOVA) with Dunn's post hoc test for multiple unpaired comparisons. \*P < 0.05; \*\*P < 0.005; \*\*\*P < 0.001; \*\*\*\*P < 0.0001.

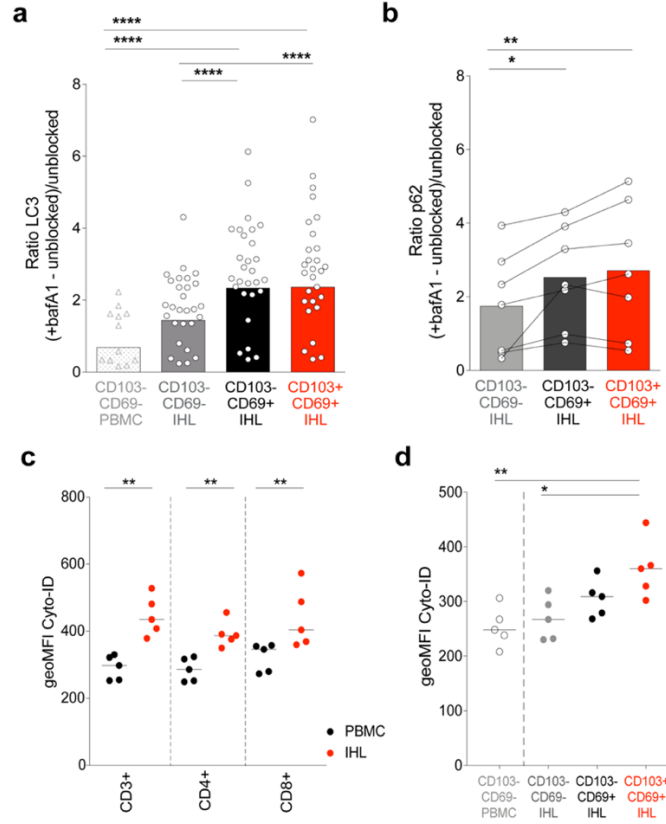


**Figure S2. Autophagic flux is highest in CD8<sup>+</sup> T<sub>RM</sub> in the liver when normalising for basal autophagy levels; Related to Figure 3; (a)** The ratio of the geoMFI of LC3 (12 biological replicates PBMC, 21 biological replicates IHL) or **(b)** p62 (Sequestosome-1, SQSTM1; 7 biological replicates) between blocked (+bafA1) and unblocked samples for liver-resident (CD69<sup>+</sup>CD103<sup>-</sup> [black] and CD69<sup>+</sup>CD103<sup>+</sup> [red] subsets) and non-resident liver infiltrating T cells (CD69<sup>-</sup>CD103<sup>-</sup> [light grey]) in the human liver and CD69<sup>-</sup>CD103<sup>-</sup> CD8<sup>+</sup> T cells in paired PBMC (LC3 only). The ratio was calculated as follows: (+bafA1 blocked geoMFI marker - unblocked geoMFI marker) / unblocked geoMFI marker. **(c-d)** Summary data for the geoMFI of Cyto-ID on **(c)** CD3<sup>+</sup>, CD4<sup>+</sup>, and CD8<sup>+</sup> T cells in thawed PBMC and IHL samples and **(d)** on liver-resident (CD69<sup>+</sup>CD103<sup>-</sup> [black] and CD69<sup>+</sup>CD103<sup>+</sup> [red] subsets) and non-resident liver infiltrating T cells (CD69<sup>-</sup>CD103<sup>-</sup> [grey]) from IHL or PBMC (white). Bars at geometric median (example histograms **Figure S1a**; 5 biological replicates). **(a, d)** Kruskal-Wallis (ANOVA) with Dunn's post hoc test for multiple unpaired comparisons (PBMC vs. IHL). **(a, b)** Friedman test (ANOVA) with Dunn's post hoc test multiple for paired comparisons (between IHL subsets). **(c)** Mann-Whitney unpaired t-test for unpaired PBMC vs. IHL. \*P < 0.05; \*\*P < 0.005; \*\*\*\*P < 0.0001.



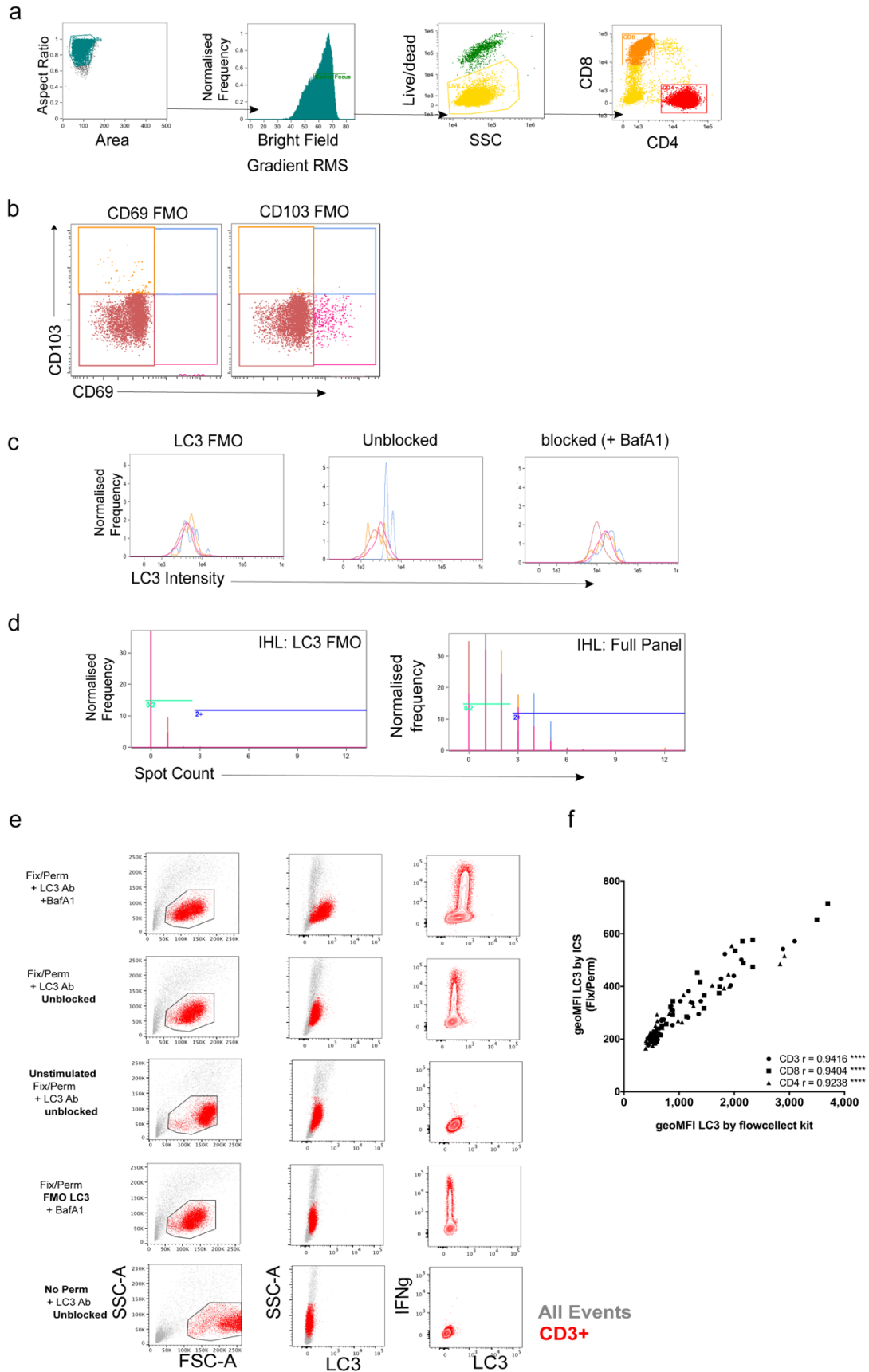


**Figure S3. Staining Controls for ImageStream and Intracellular Cytokine staining; Related to Figures 3 and 4;** **(a)** Sequential gating strategy for ImageStream data to identify: single cells (Aspect ratio vs. Area)/ cells in focus (histogram of brightfield gradient RMS)/ live cells (fixable live/dead vs. SSC)/ CD8<sup>+</sup> and CD4<sup>+</sup> T cells (CD8 vs. CD4) and **(b)** tissue-resident subsets; CD69<sup>-</sup>CD103<sup>-</sup> (red), CD69<sup>+</sup>CD103<sup>-</sup> (pink), CD69<sup>-</sup>CD103<sup>+</sup> (orange), CD69<sup>+</sup>CD103<sup>+</sup> (blue; DP). **(c)** Histograms of LC3 intensity for LC3 fluorescence minus one (FMO), unblocked (no bafilomycin A1; bafA1) and blocked (+ bafA1) showing traces for each T<sub>RM</sub> subset as shown in **(b)**; PBMC gated on CD8<sup>+</sup>). **(d)** Stacked histograms of LC3 puncta counts showing LC3 FMO (FMO) control or LC3 stained IHL (both overnight bafA1) coloured by T<sub>RM</sub> subset as in **(b)**. **(e)** Healthy human PBMC were stimulated overnight with anti-CD3/CD28 in the presence of brefeldin A. Autophagosomal degradation was blocked with bafA1 for the final 3 hours of culture. Cells were fixed (Fix/perm buffer, eBioscience TF staining kit), permeabilised (diluted 10X perm buffer, eBioscience TF staining kit), and stained with anti-human LC3 antibody (FlowCollect kit) and anti-human IFN $\gamma$  antibody (Top row). Controls were run as above but with the following changes: unblocked (no bafA1; second row); unstimulated and unblocked (no anti-CD3/CD28) to show the lack of IFN $\gamma$  staining when unstimulated (third row); unstained for anti-LC3 to show a FMO control for the FITC-labelled anti-LC3 antibody (Fourth row); unpermeabilised and unblocked to show a loss of IFN $\gamma$  and LC3 staining when cells are not permeabilised (Fifth row). Plots show SSC-A/FSC-A and SSC-A/LC3 gated on all events or CD3<sup>+</sup> (red) and IFN $\gamma$  /LC3 for CD3<sup>+</sup> T cells. **(f)** Healthy human PBMC were stimulated overnight with anti-CD3/CD28 and stained as above for intracellular cytokine staining (ICS) or they were stained according to the FlowCollect LC3 staining kit in parallel (gated on

lymphocytes/singlets/live/CD45<sup>+</sup>/pan- $\alpha\beta$  TCR<sup>+</sup>/CD3<sup>+</sup>, CD4<sup>+</sup> or CD8<sup>+</sup>; 31 biological replicates).

Spearman's rank correlation. \*\*\*P < 0.0001.

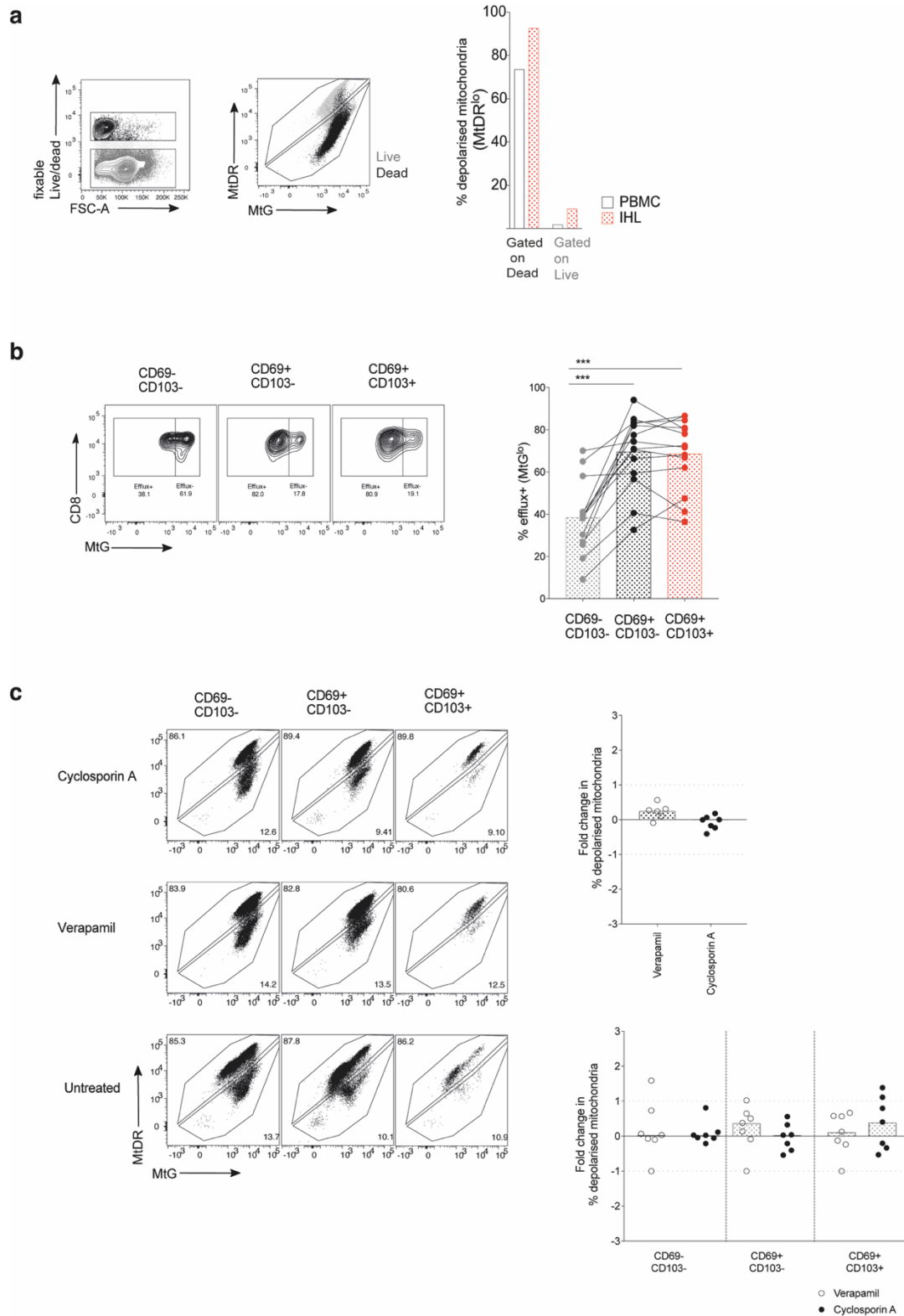


**Figure S4. Related to Figure 4e-g; Mitochondrial staining of human T cells, staining controls; (a)** Example plots of fixable live/dead stain (gated on total lymphocytes) and mitoTracker deep red (MtDR) vs. mitoTracker green (MtG) co-staining of total live (fixable live/dead-; grey) and dead (fixable live/dead+; black) peripheral CD3<sup>+</sup> T cells, and summary data for percentage of depolarised mitochondria (MtDR<sup>lo</sup>) within live or dead gate for *ex vivo* stained PBMC and IHL (bars at median, 7 biological replicates). **(b)** Example plots of efflux<sup>-</sup> (MtG<sup>hi</sup>) and efflux<sup>+</sup> (MtG<sup>lo</sup>) CD8<sup>+</sup> T cells and summary data for the percentage of efflux<sup>+</sup> T<sub>RM</sub> in *ex vivo* stained IHL (bars at mean; 14 biological replicates). **(c)** Example plots and summary data for percentage of total CD8<sup>+</sup> T cells (top) or CD8<sup>+</sup> T<sub>RM</sub> subsets (bottom) with depolarised mitochondria (MtDR<sup>lo</sup>) *ex vivo* within IHL samples after treatment with cyclosporin A (50  $\mu$ M) or verapamil (50  $\mu$ M; fold change calculated as (treated – untreated)/untreated); 6-7 biological replicates). **(b)** Friedman test (ANOVA) with Dunn's post hoc test multiple for paired comparisons (between IHL subsets). **(c)** Kruskal-Wallis (ANOVA) with Dunn's post hoc test for multiple unpaired comparisons (untreated vs. CSA vs. verapamil for total CD8<sup>+</sup> T cells and for each T<sub>RM</sub> subset). \*\*\*P < 0.001.

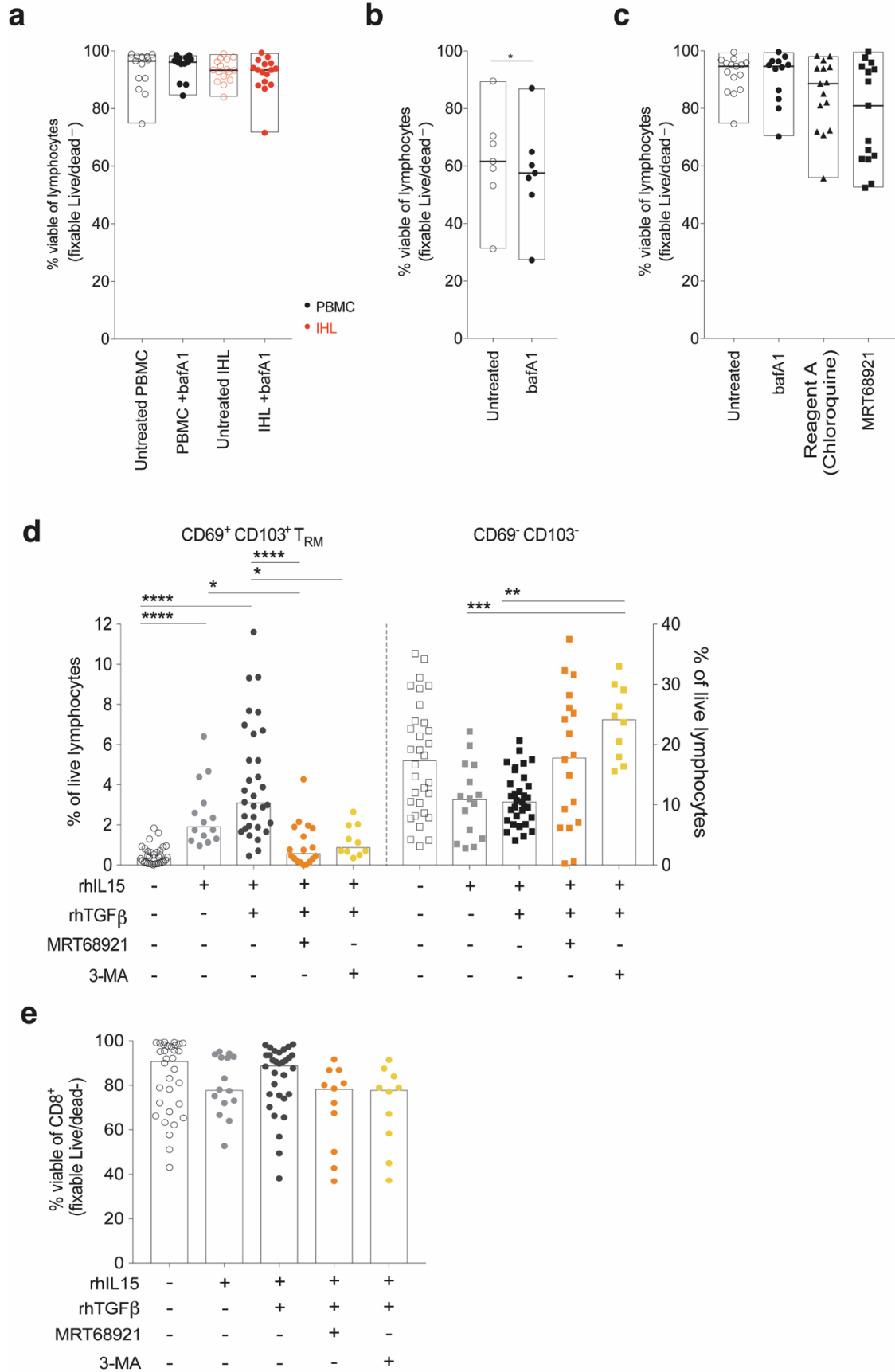


**Figure S5. Lymphocyte viability after overnight or six day culture in the presence of autophagy inhibitors; Related to Figures S1c, S2b, 4g and 5e-f;** (a) The percentage of fixable live/dead<sup>+</sup> (viable) lymphocytes in PBMC and IHL samples after overnight culture with and without bafilomycinA1 (LC3-I staining in **Figure S1c**; 13-16 biological replicates). (b) The percentage of fixable live/dead<sup>+</sup> (viable) lymphocytes in IHL samples after overnight culture with and without bafilomycinA1 (p62 staining in **Figure S2b**; 7 biological replicates). (c) The percentage of fixable live/dead<sup>+</sup> (viable) lymphocytes in PBMC and IHL samples after overnight culture with and without bafilomycinA1, Reagent A and MRT68921 dihydrochloride (MitoTracker staining in **Figure S1c**; 14-15 biological replicates). (d) The magnitude of the induced CD69<sup>+</sup>CD103<sup>+</sup> T<sub>RM</sub> or non-T<sub>RM</sub> CD69<sup>+</sup>CD103<sup>+</sup> T cell population as a percentage of total live lymphocytes and (e) the viability of total CD8<sup>+</sup> T cells after 6 days culture with sequential rhIL-15 then rhTGFβ in the presence of autophagy inhibitors: MRT68921 dihydrochloride (1 μM), and 3-MA (3-Methyladenine, 0.5 mM; 10-32 biological replicates). (a-b) Wilcoxon paired t-test between (a) untreated and bafA1 treated PBMC and IHL (related to **Figure S1c**; non-significant) and (b) untreated and bafA1 treated IHL (related to **Figure S2b**). (c-e) Kruskal-Wallis (ANOVA) with Dunn's post hoc test for multiple unpaired comparisons, untreated vs. other treatments (all non-significant; related to **Figure 4g**). \*P < 0.05; \*\*P < 0.005; \*\*\*\*P < 0.0001.

Sex	Treatment	eAb status	HBV DNA	ALT
F	Untreated	eAb+	127	20
M	Untreated	eAb+	blq	39
M	Untreated	eAb+	436	41
F	Tenofovir	eAb+	blq	27
M	Untreated	eAb+	1072	28
M	Untreated	eAb+	4,400	38
F	Untreated	eAb+	1,100,000	63
F	Untreated	eAb+	blq	nd
M	Untreated	eAb- eAg+ (low)	322	27
M	Untreated	eAb+	blq	19

**Table S1. Hepatitis-B virus infected patient characteristics. Related to Figure 3g:**

F, Female; M, Male; eAb, anti-hepatitis B virus e antigen antibodies; blq, below level of quantitation; nd, not done.

## REFERENCES

- Baumann, N.S., Torti, N., Welten, S.P.M., Barnstorf, I., Borsa, M., Pallmer, K., Oduro, J.D., Cicin-Sain, L., Ikuta, K., Ludewig, B. & Oxenius, A., 2018. Tissue maintenance of CMV-specific inflationary memory T cells by IL-15. *PLoS Pathogens*, 14(4), p.e1006993.
- Bengsch, B., Johnson, A.L., Kurachi, M., Odorizzi, P.M., Pauken, K.E., Attanasio, J., Stelekati, E., McLane, L.M., Paley, M.A., Delgoffe, G.M. & Wherry, E.J., 2016. Bioenergetic Insufficiencies Due to Metabolic Alterations Regulated by the Inhibitory Receptor PD-1 Are an Early Driver of CD8<sup>+</sup> T Cell Exhaustion. *Immunity*, 45(2), pp.358–373.
- Botbol, Y., Patel, B. & Macian, F., 2015. Common  $\gamma$ -chain cytokine signaling is required for macroautophagy induction during CD4<sup>+</sup> T-cell activation. *Autophagy*, 11(10), pp.1864–1877.

- Carreau, A., Hafny-Rahbi, B. El, Matejuk, A., Grillon, C. & Kieda, C., 2011. Why is the partial oxygen pressure of human tissues a crucial parameter? Small molecules and hypoxia. *Journal of Cellular and Molecular Medicine*, 15(6), pp.1239–1253.
- Clarke, A.J., Ellinghaus, U., Cortini, A., Stranks, A., Simon, A.K., Botto, M., Vyse, T.J. & Kvien, T.K., 2015. Autophagy is activated in systemic lupus erythematosus and required for plasmablast development. *Annals of the Rheumatic Diseases*, 74(5), pp.912–20.
- Clarke, A.J. & Simon, A.K., 2019. Autophagy in the renewal, differentiation and homeostasis of immune cells. *Nature Reviews Immunology*, 19(3), pp.170–183.
- Clarke, A.J., Riffelmacher, T., Braas, D., Cornall, R.J. & Simon, A.K., 2018. B1a B cells require autophagy for metabolic homeostasis and self-renewal. *Journal of Experimental Medicine*, 215(2), pp.399–413.
- Das, A., Hoare, M., Davies, N., Lopes, A.R., Dunn, C., Kennedy, P.T.F., Alexander, G., Finney, H., Lawson, A., Plunkett, F.J., Bertoletti, A., Akbar, A.N. & Maini, M.K., 2008. Functional skewing of the global CD8 T cell population in chronic hepatitis B virus infection. *Journal of Experimental Medicine*, 205(9), pp.2111–2124.
- DeVorkin, L., Pavey, N., Carleton, G., Comber, A., Ho, C., Lim, J., McNamara, E., Huang, H., Kim, P., Zacharias, L.G., Mizushima, N., Saitoh, T., Akira, S., Beckham, W., Lorzadeh, A., Moksa, M., Cao, Q., Murthy, A., Hirst, M., DeBerardinis, R.J. & Lum, J.J., 2019. Autophagy Regulation of Metabolism Is Required for CD8 + T Cell Anti-tumor Immunity. *Cell Reports*, 27(2), pp.502-513.e5.
- Eng, K.E., Panas, M.D., Karlsson Hedestam, G.B. & McInerney, G.M., 2010. A novel quantitative flow cytometry-based assay for autophagy. *Autophagy*, 6(5), pp.634–641.
- Fernandez-Ruiz, D., Ng, W.Y., Holz, L.E., Ma, J.Z., Zaid, A., Wong, Y.C., Lau, L.S., Mollard,



- V., Cozijnsen, A., Collins, N., Li, J., Davey, G.M., Kato, Y., Devi, S., Skandari, R., Pauley, M., Manton, J.H., Godfrey, D.I., Braun, A., Tay, S.S., Tan, P.S., Bowen, D.G., Koch-Nolte, F., Rissiek, B., Carbone, F.R., Crabb, B.S., Lahoud, M., Cockburn, I.A., Mueller, S.N., Bertolino, P., McFadden, G.I., Caminschi, I. & Heath, W.R., 2016. Liver-Resident Memory CD8<sup>+</sup> T Cells Form a Front-Line Defense against Malaria Liver-Stage Infection. *Immunity*, 45(4), pp.889–902.
- Fisicaro, P., Barili, V., Montanini, B., Acerbi, G., Ferracin, M., Guerrieri, F., Salerno, D., Boni, C., Massari, M., Cavallo, M.C., Grossi, G., Giuberti, T., Lampertico, P., Missale, G., Levrero, M., Ottonello, S. & Ferrari, C., 2017. Targeting mitochondrial dysfunction can restore antiviral activity of exhausted HBV-specific CD8 T cells in chronic hepatitis B. *Nature Medicine*, 23(3), pp.327–336.
- Foreman, K.J., Marquez, N., Dolgert, A., Fukutaki, K., Fullman, N., McGaughey, M., Pletcher, M.A., Smith, A.E., Tang, K., Yuan, C.-W., Brown, J.C., Friedman, J., He, J., Heuton, K.R., Holmberg, M., Patel, D.J., Reidy, P., Carter, A., Cercy, K., Chapin, A., Douwes-Schultz, D., Frank, T., Goettsch, F., Liu, P.Y., Nandakumar, V., Reitsma, M.B., Reuter, V., Sadat, N., Sorensen, R.J.D., Srinivasan, V., Updike, R.L., York, H., Lopez, A.D., Lozano, R., Lim, S.S., Mokdad, A.H., Vollset, S.E. & Murray, C.J.L., 2018. Forecasting life expectancy, years of life lost, and all-cause and cause-specific mortality for 250 causes of death: reference and alternative scenarios for 2016-40 for 195 countries and territories. *Lancet*, 392(10159), pp.2052–2090.
- García-Ruiz, C. & Fernández-Checa, J.C., 2018. Mitochondrial Oxidative Stress and Antioxidants Balance in Fatty Liver Disease. *Hepatology Communications*, 2(12), pp.1425–1439.

- Golden-Mason, L., Kelly, A.M., Doherty, D.G., Traynor, O., McEntee, G., Kelly, J., Hegarty, J.E. & O'Farrelly, C., 2004. Hepatic interleukin 15 (IL-15) expression: Implications for local NK/NKT cell homeostasis and development. *Clinical and Experimental Immunology*, 138(1), pp.94–101.
- Graber-Stiehl, I., 2018. The silent epidemic killing more people than HIV, malaria or TB. *Nature*, 564(7734), pp.24–26.
- Haynes, C.M., Fiorese, C.J. & Lin, Y.F., 2013. Evaluating and responding to mitochondrial dysfunction: The mitochondrial unfolded-protein response and beyond. *Trends in Cell Biology*, 23(7), pp.311–318.
- Hernandezgea, V., Ghiassinejad, Z., Rozenfeld, R., Gordon, R., Fiel, M.I., Yue, Z., Czaja, M.J. & Friedman, S.L., 2012. Autophagy releases lipid that promotes fibrogenesis by activated hepatic stellate cells in mice and in human tissues. *Gastroenterology*, 142(4), pp.938–946.
- Holz, L.E., Prier, J.E., Freestone, D., Steiner, T.M., English, K., Johnson, D.N., Mollard, V., Cozijnsen, A., Davey, G.M., Godfrey, D.I., Yui, K., Mackay, L.K., Lahoud, M.H., Caminschi, I., McFadden, G.I., Bertolino, P., Fernandez-Ruiz, D. & Heath, W.R., 2018. CD8<sup>+</sup> T Cell Activation Leads to Constitutive Formation of Liver Tissue-Resident Memory T Cells that Seed a Large and Flexible Niche in the Liver. *Cell Reports*, 25(1), pp.68-79.e4.
- Huang, W.-C., Easom, N.J., Tang, X.-Z., Gill, U.S., Singh, H., Robertson, F., Chang, C., Trowsdale, J., Davidson, B.R., Rosenberg, W.M., Fusai, G., Toubert, A., Kennedy, P.T., Peppas, D. & Maini, M.K., 2017. T Cells Infiltrating Diseased Liver Express Ligands for the NKG2D Stress Surveillance System. *The Journal of Immunology*, 198(3), pp.1172–1182.
- Hubbard, V.M., Valdor, R., Patel, B., Singh, R., Cuervo, A.M. & Macian, F., 2010. Macroautophagy Regulates Energy Metabolism during Effector T Cell Activation. *The*

- Journal of Immunology*, 185(12), pp.7349–7357.
- Hurton, L. V., Singh, H., Najjar, A.M., Switzer, K.C., Mi, T., Maiti, S., Olivares, S., Rabinovich, B., Huls, H., Forget, M.A., Datar, V., Kebriaei, P., Lee, D.A., Champlin, R.E. & Cooper, L.J.N., 2016. Tethered IL-15 augments antitumor activity and promotes a stem-cell memory subset in tumor-specific T cells. *Proceedings of the National Academy of Sciences of the United States of America*, 113(48), pp.E7788–E7797.
- Jia, W. & He, Y.-W., 2011. Temporal regulation of intracellular organelle homeostasis in T lymphocytes by autophagy. *The Journal of Immunology*, 186(9), pp.5313–5322.
- Jiao, J., Ooka, K., Fey, H., Fiel, M.I., Rahmman, A.H., Kojima, K., Hoshida, Y., Chen, X., de Paula, T., Vetter, D., Sastre, D., Lee, K.H., Lee, Y.A., Bansal, M., Friedman, S.L., Merad, M. & Aloman, C., 2016. Interleukin-15 receptor  $\alpha$  on hepatic stellate cells regulates hepatic fibrogenesis in mice. *Journal of Hepatology*, 65(2), pp.344–353.
- Kabat, A.M., Harrison, O.J., Riffelmacher, T., Moghaddam, A.E., Pearson, C.F., Laing, A., Abeler-Dörner, L., Forman, S.P., Grecis, R.K., Sattentau, Q., Simon, A.K., Pott, J. & Maloy, K.J., 2016. The autophagy gene Atg16l1 differentially regulates Treg and TH2 cells to control intestinal inflammation. *eLife*, 5, p.e12444.
- Klionsky, D.J., Abdelmohsen, K., Abe, A., Abedin, M.J., Abeliovich, H., ... Bumbasi..., 2016. Guidelines for the use and interpretation of assays for monitoring autophagy (3rd edition). *Autophagy*, 12(1), pp.1–222.
- Kumar, B. V., Kratchmarov, R., Miron, M., Carpenter, D.J., Senda, T., Lerner, H., Friedman, A., Reiner, S.L. & Farber, D.L., 2018. Functional heterogeneity of human tissue-resident memory T cells based on dye efflux capacities. *JCI insight*, 3(22).
- Mackay, L.K., Wynne-Jones, E., Freestone, D., Pellicci, D.G., Mielke, L.A., Newman, D.M.,

- Braun, A., Masson, F., Kallies, A., Belz, G.T. & Carbone, F.R., 2015. T-box Transcription Factors Combine with the Cytokines TGF- $\beta$  and IL-15 to Control Tissue-Resident Memory T Cell Fate. *Immunity*, 43(6), pp.1101–1111.
- Maini, M.K. & Pallett, L.J., 2018. Defective T-cell immunity in hepatitis B virus infection: why therapeutic vaccination needs a helping hand. *The Lancet Gastroenterology and Hepatology*, 3(3), pp.192–202.
- Mocholi, E., Dowling, S.D., Botbol, Y., Gruber, R.C., Ray, A.K., Vastert, S., Shafit-Zagardo, B., Coffey, P.J. & Macian, F., 2018. Autophagy Is a Tolerance-Avoidance Mechanism that Modulates TCR-Mediated Signaling and Cell Metabolism to Prevent Induction of T Cell Anergy. *Cell Reports*, 24(5), pp.1136–1150.
- Murera, D., Arbogast, F., Arnold, J., Bouis, D., Muller, S. & Gros, F., 2018. CD4 T cell autophagy is integral to memory maintenance. *Scientific Reports*, 8(1), p.696.
- O’Sullivan, T.E., Geary, C.D., Weizman, O. El, Geiger, T.L., Rapp, M., Dorn, G.W., Overholtzer, M. & Sun, J.C., 2016. Atg5 Is Essential for the Development and Survival of Innate Lymphocytes. *Cell Reports*, 15(9), pp.1910–1919.
- Pallett, L.J., Davies, J., Colbeck, E.J., Robertson, F., Hansi, N., Easom, N.J.W., Burton, A.R., Stegmann, K.A., Schurich, A., Swadling, L., Gill, U.S., Male, V., Luong, T.V., Gander, A., Davidson, B.R., Kennedy, P.T.F. & Maini, M.K., 2017. IL-2high tissue-resident T cells in the human liver: Sentinels for hepatotropic infection. *Journal of Experimental Medicine*, 214(6), pp.1567–1580.
- Pallett, L.J., Gill, U.S., Quaglia, A., Sinclair, L. V., Jover-Cobos, M., Schurich, A., Singh, K.P., Thomas, N., Das, A., Chen, A., Fusai, G., Bertolotti, A., Cantrell, D.A., Kennedy, P.T., Davies, N.A., Haniffa, M. & Maini, M.K., 2015. Metabolic regulation of hepatitis B

- immunopathology by myeloid-derived suppressor cells. *Nature Medicine*, 21(6), pp.591–600.
- Petherick, K.J., Conway, O.J.L., Mpamhanga, C., Osborne, S.A., Kamal, A., Saxty, B. & Ganley, I.G., 2015. Pharmacological inhibition of ULK1 kinase blocks mammalian target of rapamycin (mTOR)-dependent autophagy. *Journal of Biological Chemistry*, 290(18), pp.11376–11383.
- Phadwal, K., Alegre-Abarategui, J., Watson, A.S., Pike, L., Anbalagan, S., Hammond, E.M., Wade-Martins, R., McMichael, A., Klenerman, P. & Simon, A.K., 2012. A novel method for autophagy detection in primary cells Impaired levels of macroautophagy in immunosenescent T cells. *Autophagy*, 8(4), pp.677–689.
- Pilipow, K., Roberto, A., Roederer, M., Waldmann, T.A., Mavilio, D. & Lugli, E., 2015. IL15 and T-cell stemness in T-cell-based cancer immunotherapy. *Cancer Research*, 75(24), pp.5187–5193.
- Protzer, U., Maini, M.K. & Knolle, P.A., 2012. Living in the liver: Hepatic infections. *Nature Reviews Immunology*, 12(3), pp.201–213.
- Pua, H.H., Dzhagalov, I., Chuck, M., Mizushima, N. & He, Y.-W., 2007. A critical role for the autophagy gene Atg5 in T cell survival and proliferation. *The Journal of experimental medicine*, 204(1), pp.25–31.
- Pua, H.H., Guo, J., Komatsu, M. & He, Y.-W., 2009. Autophagy Is Essential for Mitochondrial Clearance in Mature T Lymphocytes. *The Journal of Immunology*, 182(7), pp.4046–4055.
- Puleston, D., 2015. Detection of mitochondrial mass, damage, and reactive oxygen species by flow cytometry. *Cold Spring Harbor Protocols*, 2015(9), pp.830–834.
- Puleston, D.J., Zhang, H., Powell, T.J., Lipina, E., Sims, S., Panse, I., Watson, A.S., Cerundolo,

- V., Townsend, A.R.M., Klenerman, P. & Simon, A.K., 2014. Autophagy is a critical regulator of memory CD8<sup>+</sup> T cell formation. *eLife*, 3, pp.1–21.
- Qasim, W., Brunetto, M., Gehring, A.J., Xue, S.A., Schurich, A., Khakpoor, A., Zhan, H., Ciccorossi, P., Gilmour, K., Cavallone, D., Moriconi, F., Farzhenah, F., Mazzoni, A., Chan, L., Morris, E., Thrasher, A., Maini, M.K., Bonino, F., Stauss, H. & Bertoletti, A., 2015. Immunotherapy of HCC metastases with autologous T cell receptor redirected T cells, targeting HBsAg in a liver transplant patient. *Journal of Hepatology*, 62(2), pp.486–491.
- Riffelmacher, T., Richter, F.C. & Simon, A.K., 2018. Autophagy dictates metabolism and differentiation of inflammatory immune cells. *Autophagy*, 14(2), pp.199–206.
- Sallusto, F., Lenig, D., Förster, R., Lipp, M. & Lanzavecchia, A., 1999. Two subsets of memory T lymphocytes with distinct homing potentials and effector functions. *Nature*, 401(6754), pp.708–712.
- Salou, M., Legoux, F., Gilet, J., Darbois, A., Du Halgouet, A., Alonso, R., Richer, W., Goubet, A.G., Daviaud, C., Menger, L., Procopio, E., Premel, V. & Lantz, O., 2019. A common transcriptomic program acquired in the thymus defines tissue residency of MAIT and NKT subsets. *Journal of Experimental Medicine*, 216(1), pp.133–151.
- Sanderson, S.L. & Simon, A.K., 2017. In aged primary T cells, mitochondrial stress contributes to telomere attrition measured by a novel imaging flow cytometry assay. *Aging Cell*, 16(6), pp.1234–1243.
- Di Scala, M., Otano, I., Gil-Fariña, I., Vanrell, L., Hommel, M., Olagüe, C., Vales, A., Galarraga, M., Guembe, L., Ortiz de Solorzano, C., Ghosh, I., Maini, M.K., Prieto, J. & González-Aseguinolaza, G., 2016. Complementary Effects of Interleukin-15 and Alpha Interferon Induce Immunity in Hepatitis B Virus Transgenic Mice. *Journal of Virology*,

90(19), pp.8563–8574.

- Schlie, K., Westerback, A., DeVorkin, L., Hughson, L.R., Brandon, J.M., MacPherson, S., Gadawski, I., Townsend, K.N., Poon, V.I., Elrick, M.A., Côté, H.C.F., Abraham, N., Wherry, E.J., Mizushima, N. & Lum, J.J., 2015. Survival of Effector CD8 + T Cells during Influenza Infection Is Dependent on Autophagy . *The Journal of Immunology*, 194(9), pp.4277–4286.
- Schurich, A., Pallett, L.J., Jajbhay, D., Wijngaarden, J., Otano, I., Gill, U.S., Hansi, N., Kennedy, P.T., Nastouli, E., Gilson, R., Frezza, C., Henson, S.M. & Maini, M.K., 2016. Distinct Metabolic Requirements of Exhausted and Functional Virus-Specific CD8 T Cells in the Same Host. *Cell Reports*, 16(5), pp.1243–1252.
- Sowell, R.T., Goldufsky, J.W., Rogozinska, M., Quiles, Z., Cao, Y., Castillo, E.F., Finnegan, A. & Marzo, A.L., 2017. IL-15 Complexes Induce Migration of Resting Memory CD8 T Cells into Mucosal Tissues. *The Journal of Immunology*, 199(7), pp.2536–2546.
- Stelma, F., van der Ree, M.H., Sinnige, M.J., Brown, A., Swadling, L., de Vree, J.M.L., Willemse, S.B., van der Valk, M., Grint, P., Neben, S., Klenerman, P., Barnes, E., Kootstra, N.A. & Reesink, H.W., 2017. Immune phenotype and function of natural killer and T cells in chronic hepatitis C patients who received a single dose of anti-MicroRNA-122, RG-101. *Hepatology*, 66(1), pp.57–68.
- Stephenson, L.M., Miller, B.C., Ng, A., Eisenberg, J., Zhao, Z., Cadwell, K., Graham, D.B., Mizushima, N.N., Xavier, R., Virgin, H.W. & Swat, W., 2009. Identification of Atg5-dependent transcriptional changes and increases in mitochondrial mass in Atg5-deficient T lymphocytes. *Autophagy*, 5(5), pp.625–635.
- Tse, S.-W.W., Radtke, A.J. & Zavala, F., 2011. Induction and maintenance of protective CD8+ T

- cells against malaria liver stages: implications for vaccine development. *Memórias do Instituto Oswaldo Cruz*, 106, pp.172–178.
- Villa, E., Marchetti, S. & Ricci, J.E., 2018. No Parkin Zone: Mitophagy without Parkin. *Trends in Cell Biology*, 28(11), pp.882–895.
- Watanabe, R., Fujii, H., Shirai, T., Saito, S., Ishii, T. & Harigae, H., 2014. Autophagy plays a protective role as an anti-oxidant system in human T cells and represents a novel strategy for induction of T-cell apoptosis. *European Journal of Immunology*, 44(8), pp.2508–2520.
- Winau, F., Hegasy, G., Weiskirchen, R., Weber, S., Cassan, C., Sieling, P.A., Modlin, R.L., Liblau, R.S., Gressner, A.M. & Kaufmann, S.H.E., 2007. Ito Cells Are Liver-Resident Antigen-Presenting Cells for Activating T Cell Responses. *Immunity*, 26(1), pp.117–129.
- Wu, Y.T., Tan, H.L., Shui, G., Bauvy, C., Huang, Q., Wenk, M.R., Ong, C.N., Codogno, P. & Shen, H.M., 2010. Dual role of 3-methyladenine in modulation of autophagy via different temporal patterns of inhibition on class I and III phosphoinositide 3-kinase. *Journal of Biological Chemistry*, 285(14), pp.10850–10861.
- Xu, X., Araki, K., Li, S., Han, J.H., Ye, L., Tan, W.G., Konieczny, B.T., Bruinsma, M.W., Martinez, J., Pearce, E.L., Green, D.R., Jones, D.P., Virgin, H.W. & Ahmed, R., 2014. Autophagy is essential for effector CD8 + T cell survival and memory formation. *Nature Immunology*, 15(12), pp.1152–1161.
- Yang, Z., Fujii, H., Mohan, S. V, Goronzy, J.J. & Weyand, C.M., 2013. Phosphofructokinase deficiency impairs ATP generation, autophagy, and redox balance in rheumatoid arthritis T cells. *The Journal of experimental medicine*, 210(10), pp.2119–2134.
- Zeng, R., Spolski, R., Finkelstein, S.E., Oh, S.K., Kovanen, P.E., Hinrichs, C.S., Pise-Masison, C.A., Radonovich, M.F., Brady, J.N., Restifo, N.P., Berzofsky, J.A. & Leonard, W.J., 2005.



- Synergy of IL-21 and IL-15 in regulating CD8<sup>+</sup> T cell expansion and function. *Journal of Experimental Medicine*, 201(1), pp.139–148.
- Zhou, Z., Xu, M.J., Cai, Y., Wang, W., Jiang, J.X., Varga, Z. V., Feng, D., Pacher, P., Kunos, G., Torok, N.J. & Gao, B., 2018. Neutrophil–Hepatic Stellate Cell Interactions Promote Fibrosis in Experimental Steatohepatitis. *Cmgh*, 5(3), pp.399–413.
- Zhu, L., Xie, X., Zhang, L., Wang, H., Jie, Z., Zhou, X., Shi, J., Zhao, S., Zhang, B., Cheng, X. & Sun, S.C., 2018. TBK-binding protein 1 regulates IL-15-induced autophagy and NKT cell survival. *Nature Communications*, 9(1).
- Zinser, M.E., Highton, A.J., Kurioka, A., Kronsteiner, B., Hagel, J., Leng, T., Marchi, E., Phetsouphanh, C., Willberg, C.B., Dunachie, S.J. & Klenerman, P., 2018. Human MAIT cells show metabolic quiescence with rapid glucose-dependent upregulation of granzyme B upon stimulation. *Immunology and Cell Biology*, 117, p.1250.

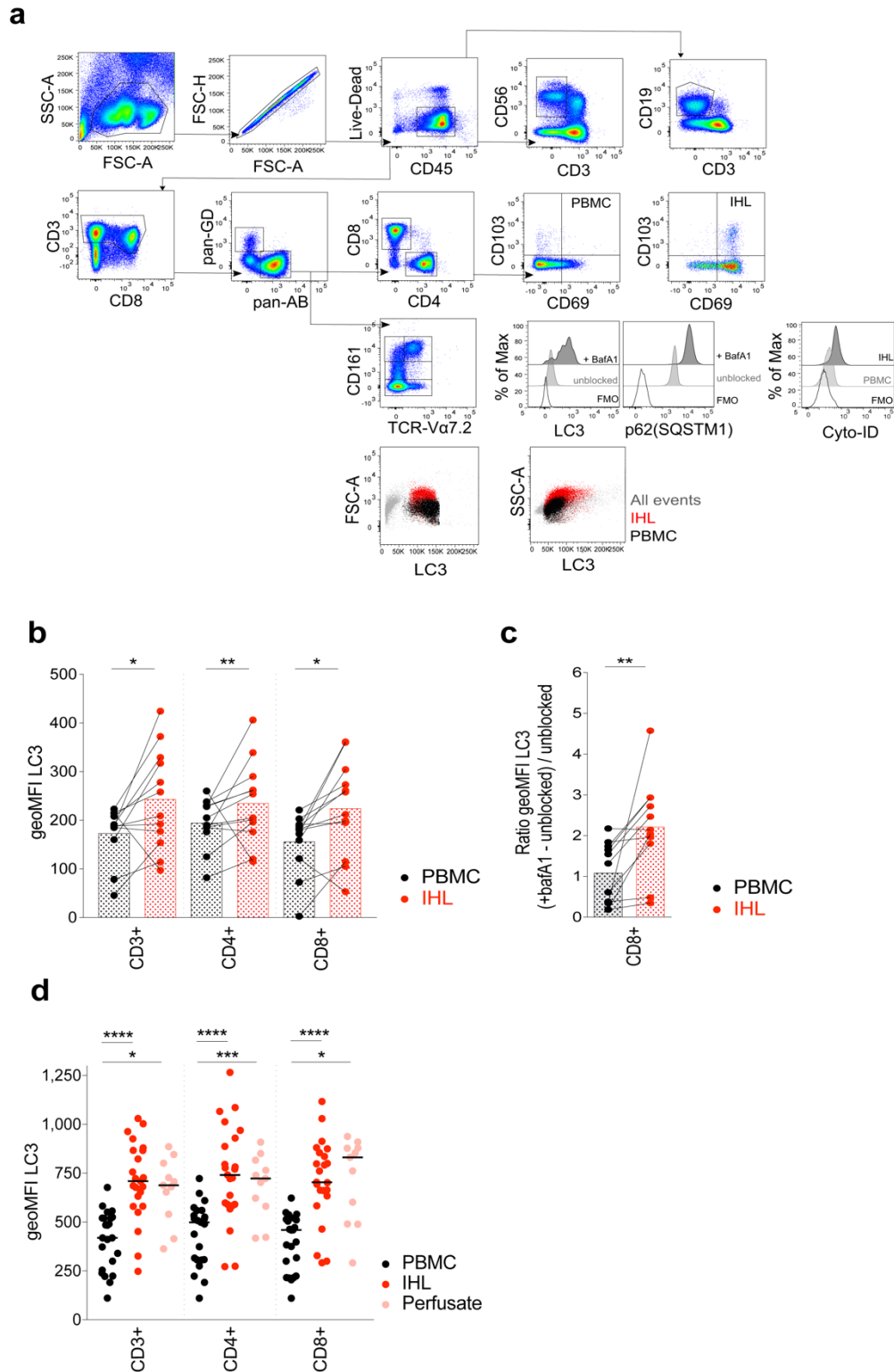


**Figure S1. Sequential gating strategy for lymphocyte subsets and LC3 liver staining controls; Related to Figure 1; (a) Sequential gating strategy to identify: lymphocytes (SSC-A**

vs. FSC-A)/single cells (FSC-H vs. FSC-A)/live CD45<sup>+</sup> lymphocytes (Fixable live/dead<sup>-</sup> CD45<sup>+</sup>)/NK cells (CD56<sup>+</sup> CD3<sup>-</sup>), B cells (CD19<sup>+</sup> CD3<sup>-</sup>), T cells (CD3<sup>+</sup>)/pan- $\gamma\delta$  and pan- $\alpha\beta$  T cells (pan- $\gamma\delta$  TCR vs. pan- $\alpha\beta$  TCR)/MAITs (CD161<sup>hi</sup> TCR-V $\alpha$  7.2<sup>+</sup>) and CD161mids (CD161<sup>mid</sup> TCR-V $\alpha$  7.2<sup>-</sup>), CD4<sup>+</sup> and CD8<sup>+</sup> T cells (CD4 vs. CD8)/tissue-resident T cells (CD103 vs. CD69; shown for PBMC and IHL). Also shown are example histograms of LC3 and p62 (Sequestosome-1, SQSTM1) staining of IHL treated with bafilomycin A1 (bafA1) overnight or untreated (DMSO vehicle), and Cyto-ID staining of IHL and PBMC, all gated on CD8<sup>+</sup> T cells with example fluorescence minus one stains (FMO). FSC-A vs. LC3 and SSC-A vs. LC3 plots are shown for all events (grey), CD3<sup>+</sup> T cells in PBMC (black) and CD3<sup>+</sup> T cells in IHL (red), showing a higher LC3 staining for cells of equivalent size and granularity in IHL samples relative to PBMC samples. **(b)** Summary data of the geoMFI of LC3 on CD3<sup>+</sup>, CD4<sup>+</sup>, and CD8<sup>+</sup> T cells in paired PBMC and IHL samples *ex vivo* without bafA1 treatment (unblocked; bars at mean; 12 biological replicates). **(c)** The ratio of geoMFI LC3 between accumulated (blocked; + bafA1) and basal (unblocked) samples for CD8<sup>+</sup> T cells from paired PBMC and IHL samples calculated as follows: (geoMFI LC3 with bafA1 – unblocked geoMFI LC3) / unblocked geoMFI LC3; 11 biological replicates). **(d)** Summary data for CD3<sup>+</sup>, CD4<sup>+</sup>, and CD8<sup>+</sup> T cells in perfusion fluid (perfusate) and paired PBMC and IHL samples *ex vivo*. bafA1 treated (23 biological replicates for paired blood and IHL, 11 biological replicates for perfusates). **(b, c)** Wilcoxon paired t-tests. **(d)** Kruskal-Wallis (ANOVA) with Dunn's post hoc test for multiple unpaired comparisons. \*P < 0.05; \*\*P < 0.005; \*\*\*P < 0.001; \*\*\*\*P < 0.0001.

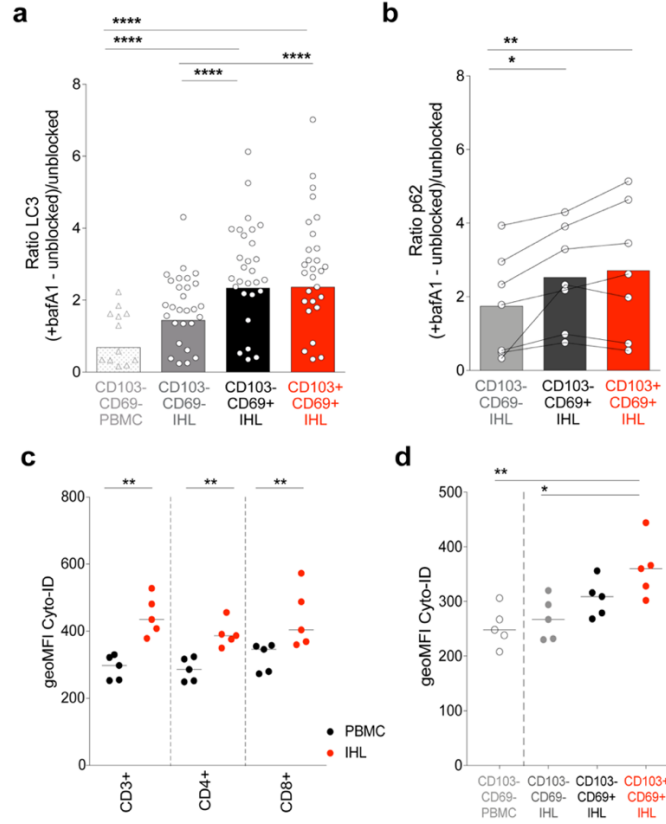


**Figure S2. Autophagic flux is highest in CD8<sup>+</sup> T<sub>RM</sub> in the liver when normalising for basal autophagy levels; Related to Figure 3; (a)** The ratio of the geoMFI of LC3 (12 biological replicates PBMC, 21 biological replicates IHL) or **(b)** p62 (Sequestosome-1, SQSTM1; 7 biological replicates) between blocked (+bafA1) and unblocked samples for liver-resident (CD69<sup>+</sup>CD103<sup>-</sup> [black] and CD69<sup>+</sup>CD103<sup>+</sup> [red] subsets) and non-resident liver infiltrating T cells (CD69<sup>-</sup>CD103<sup>-</sup> [light grey]) in the human liver and CD69<sup>-</sup>CD103<sup>-</sup> CD8<sup>+</sup> T cells in paired PBMC (LC3 only). The ratio was calculated as follows: (+bafA1 blocked geoMFI marker - unblocked geoMFI marker) / unblocked geoMFI marker. **(c-d)** Summary data for the geoMFI of Cyto-ID on **(c)** CD3<sup>+</sup>, CD4<sup>+</sup>, and CD8<sup>+</sup> T cells in thawed PBMC and IHL samples and **(d)** on liver-resident (CD69<sup>+</sup>CD103<sup>-</sup> [black] and CD69<sup>+</sup>CD103<sup>+</sup> [red] subsets) and non-resident liver infiltrating T cells (CD69<sup>-</sup>CD103<sup>-</sup> [grey]) from IHL or PBMC (white). Bars at geometric median (example histograms **Figure S1a**; 5 biological replicates). **(a, d)** Kruskal-Wallis (ANOVA) with Dunn's post hoc test for multiple unpaired comparisons (PBMC vs. IHL). **(a, b)** Friedman test (ANOVA) with Dunn's post hoc test multiple for paired comparisons (between IHL subsets). **(c)** Mann-Whitney unpaired t-test for unpaired PBMC vs. IHL. \*P < 0.05; \*\*P < 0.005; \*\*\*\*P < 0.0001.

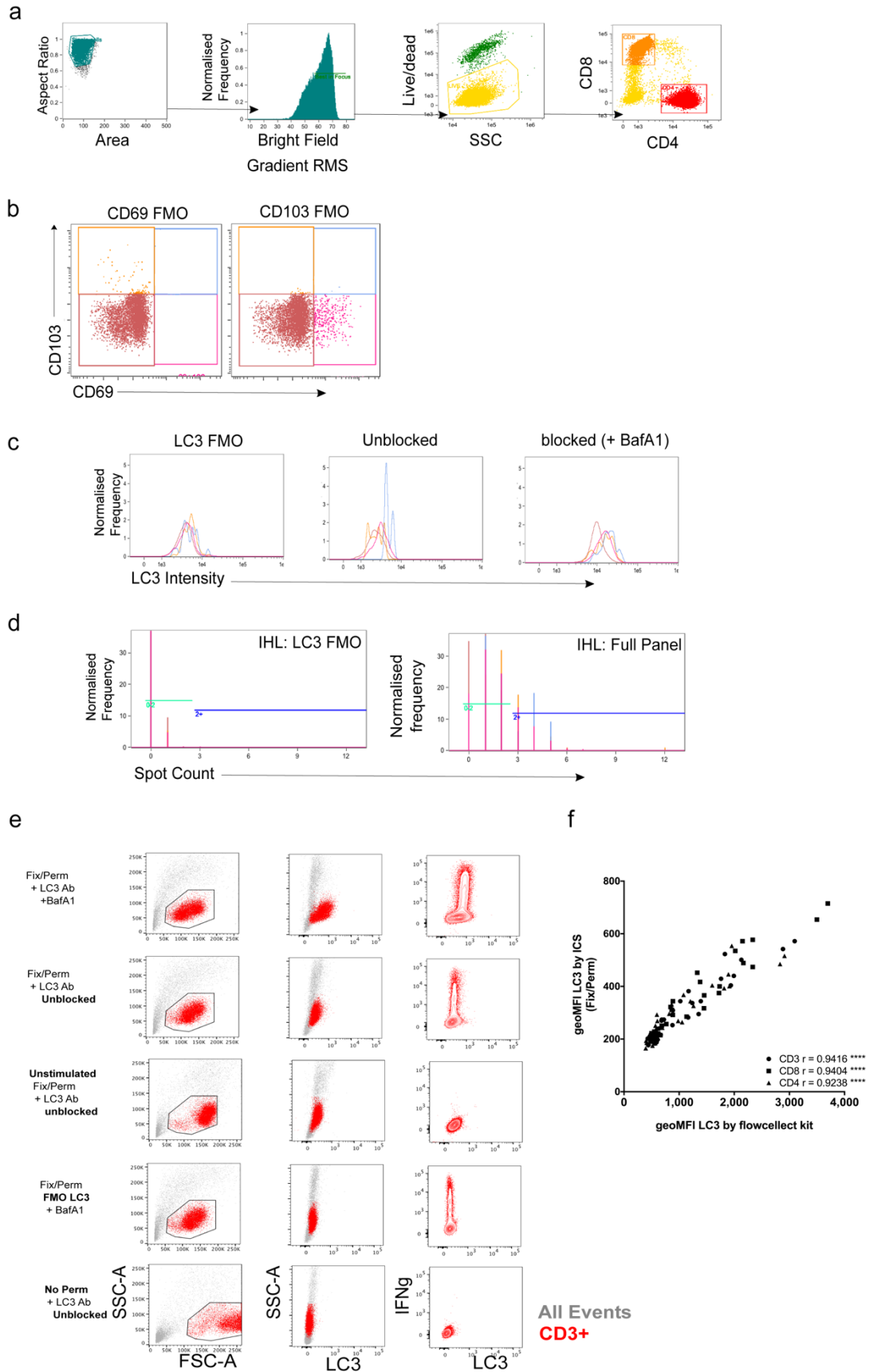


**Figure S3. Staining Controls for ImageStream and Intracellular Cytokine staining; Related to Figures 3 and 4;** (a) Sequential gating strategy for ImageStream data to identify: single cells (Aspect ratio vs. Area)/ cells in focus (histogram of brightfield gradient RMS)/ live cells (fixable live/dead vs. SSC)/ CD8<sup>+</sup> and CD4<sup>+</sup> T cells (CD8 vs. CD4) and (b) tissue-resident subsets; CD69<sup>-</sup>CD103<sup>-</sup> (red), CD69<sup>+</sup>CD103<sup>-</sup> (pink), CD69<sup>-</sup>CD103<sup>+</sup> (orange), CD69<sup>+</sup>CD103<sup>+</sup> (blue; DP). (c) Histograms of LC3 intensity for LC3 fluorescence minus one (FMO), unblocked (no bafilomycin A1; bafA1) and blocked (+ bafA1) showing traces for each T<sub>RM</sub> subset as shown in (b; PBMC gated on CD8<sup>+</sup>). (d) Stacked histograms of LC3 puncta counts showing LC3 FMO (FMO) control or LC3 stained IHL (both overnight bafA1) coloured by T<sub>RM</sub> subset as in (b). (e) Healthy human PBMC were stimulated overnight with anti-CD3/CD28 in the presence of brefeldin A. Autophagosomal degradation was blocked with bafA1 for the final 3 hours of culture. Cells were fixed (Fix/perm buffer, eBioscience TF staining kit), permeabilised (diluted 10X perm buffer, eBioscience TF staining kit), and stained with anti-human LC3 antibody (FlowCollect kit) and anti-human IFN $\gamma$  antibody (Top row). Controls were run as above but with the following changes: unblocked (no bafA1; second row); unstimulated and unblocked (no anti-CD3/CD28) to show the lack of IFN $\gamma$  staining when unstimulated (third row); unstained for anti-LC3 to show a FMO control for the FITC-labelled anti-LC3 antibody (Fourth row); unpermeabilised and unblocked to show a loss of IFN $\gamma$  and LC3 staining when cells are not permeabilised (Fifth row). Plots show SSC-A/FSC-A and SSC-A/LC3 gated on all events or CD3<sup>+</sup> (red) and IFN $\gamma$  /LC3 for CD3<sup>+</sup> T cells. (f) Healthy human PBMC were stimulated overnight with anti-CD3/CD28 and stained as above for intracellular cytokine staining (ICS) or they were stained according to the FlowCollect LC3 staining kit in parallel (gated on

lymphocytes/singlets/live/CD45<sup>+</sup>/pan- $\alpha\beta$  TCR<sup>+</sup>/CD3<sup>+</sup>, CD4<sup>+</sup> or CD8<sup>+</sup>; 31 biological replicates).

Spearman's rank correlation. \*\*\*P < 0.0001.

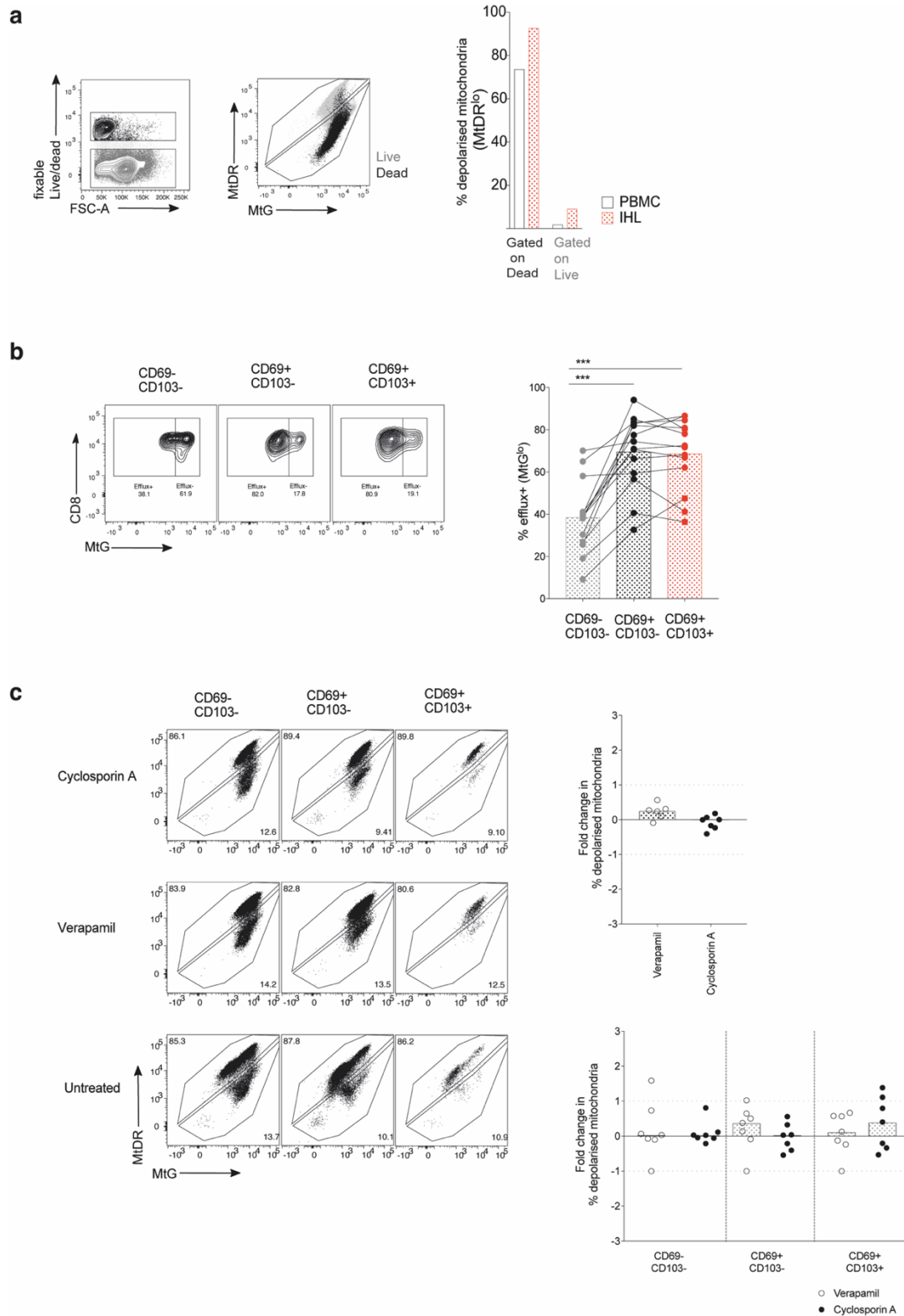


**Figure S4. Related to Figure 4e-g; Mitochondrial staining of human T cells, staining controls;** **(a)** Example plots of fixable live/dead stain (gated on total lymphocytes) and mitoTracker deep red (MtDR) vs. mitoTracker green (MtG) co-staining of total live (fixable live/dead-; grey) and dead (fixable live/dead+; black) peripheral CD3<sup>+</sup> T cells, and summary data for percentage of depolarised mitochondria (MtDR<sup>lo</sup>) within live or dead gate for *ex vivo* stained PBMC and IHL (bars at median, 7 biological replicates). **(b)** Example plots of efflux<sup>-</sup> (MtG<sup>hi</sup>) and efflux<sup>+</sup> (MtG<sup>lo</sup>) CD8<sup>+</sup> T cells and summary data for the percentage of efflux<sup>+</sup> T<sub>RM</sub> in *ex vivo* stained IHL (bars at mean; 14 biological replicates). **(c)** Example plots and summary data for percentage of total CD8<sup>+</sup> T cells (top) or CD8<sup>+</sup> T<sub>RM</sub> subsets (bottom) with depolarised mitochondria (MtDR<sup>lo</sup>) *ex vivo* within IHL samples after treatment with cyclosporin A (50  $\mu$ M) or verapamil (50  $\mu$ M; fold change calculated as (treated – untreated)/untreated); 6-7 biological replicates). **(b)** Friedman test (ANOVA) with Dunn's post hoc test multiple for paired comparisons (between IHL subsets). **(c)** Kruskal-Wallis (ANOVA) with Dunn's post hoc test for multiple unpaired comparisons (untreated vs. CSA vs. verapamil for total CD8<sup>+</sup> T cells and for each T<sub>RM</sub> subset). \*\*\*P < 0.001.



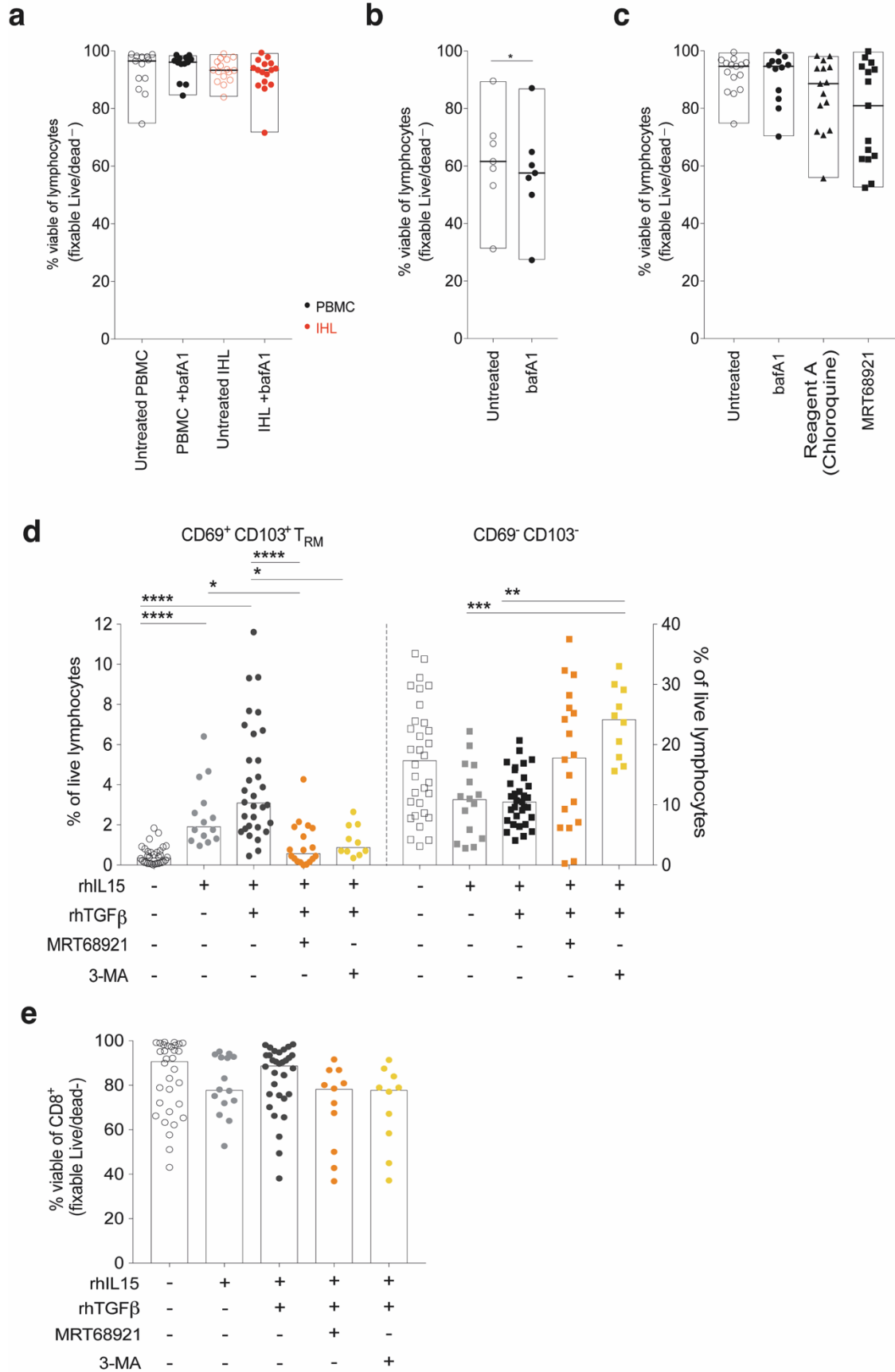


**Figure S5. Lymphocyte viability after overnight or six day culture in the presence of autophagy inhibitors; Related to Figures S1c, S2b, 4g and 5e-f;** (a) The percentage of fixable live/dead<sup>+</sup> (viable) lymphocytes in PBMC and IHL samples after overnight culture with and without bafilomycinA1 (LC3-I staining in **Figure S1c**; 13-16 biological replicates). (b) The percentage of fixable live/dead<sup>+</sup> (viable) lymphocytes in IHL samples after overnight culture with and without bafilomycinA1 (p62 staining in **Figure S2b**; 7 biological replicates). (c) The percentage of fixable live/dead<sup>+</sup> (viable) lymphocytes in PBMC and IHL samples after overnight culture with and without bafilomycinA1, Reagent A and MRT68921 dihydrochloride (MitoTracker staining in **Figure S1c**; 14-15 biological replicates). (d) The magnitude of the induced CD69<sup>+</sup>CD103<sup>+</sup> T<sub>RM</sub> or non-T<sub>RM</sub> CD69<sup>+</sup>CD103<sup>+</sup> T cell population as a percentage of total live lymphocytes and (e) the viability of total CD8<sup>+</sup> T cells after 6 days culture with sequential rhIL-15 then rhTGFβ in the presence of autophagy inhibitors: MRT68921 dihydrochloride (1 μM), and 3-MA (3-Methyladenine, 0.5 mM; 10-32 biological replicates). (a-b) Wilcoxon paired t-test between (a) untreated and bafA1 treated PBMC and IHL (related to **Figure S1c**; non-significant) and (b) untreated and bafA1 treated IHL (related to **Figure S2b**). (c-e) Kruskal-Wallis (ANOVA) with Dunn's post hoc test for multiple unpaired comparisons, untreated vs. other treatments (all non-significant; related to **Figure 4g**). \*P < 0.05; \*\*P < 0.005; \*\*\*\*P < 0.0001.

Sex	Treatment	eAb status	HBV DNA	ALT
F	Untreated	eAb+	127	20
M	Untreated	eAb+	blq	39
M	Untreated	eAb+	436	41
F	Tenofovir	eAb+	blq	27
M	Untreated	eAb+	1072	28
M	Untreated	eAb+	4,400	38
F	Untreated	eAb+	1,100,000	63
F	Untreated	eAb+	blq	nd
M	Untreated	eAb- eAg+ (low)	322	27
M	Untreated	eAb+	blq	19

**Table S1. Hepatitis-B virus infected patient characteristics. Related to Figure 3g:**

F, Female; M, Male; eAb, anti-hepatitis B virus e antigen antibodies; blq, below level of quantitation; nd, not done.